IEEE Access
Multidisciplinary ⋮ Rapid Review ⋮ Open Access Journal

Received March 25, 2020, accepted April 13, 2020, date of publication April 16, 2020, date of current version May 1, 2020.

Digital Object Identifier 10.1109/ACCESS.2020.2988323

A Data-Driven-Based Fault Diagnosis Approach for Electrical Power DC-DC Inverter by Using Modified Convolutional Neural Network With Global Average Pooling and 2-D Feature Image

WENFENG GONG[1,2], HUI CHEN[1], ZEHUI ZHANG[3], MEILING ZHANG[2], AND HAIBO GAO[1]

[1]Key Laboratory of High-Performance Ship Technology of Ministry of Education in China, School of Energy and Power Engineering, Wuhan University of Technology, Wuhan 430063, China
[2]Beihai Campus, Guilin University of Electronic and Technology, Beihai 536000, China
[3]College of Software, Nankai University, Tianjin 300350, China

Corresponding authors: Hui Chen (hchen@whut.edu.cn) and Meiling Zhang (zhangmeilingcn@163.com)

This work was supported in part by the National Natural Science Foundation of China (Research on the Electrical Propulsion Ship Electromechanical Multi-Scale Coupling and Control Method Optimization) under Grant 51579200, in part by NSFC-Zhejiang Joint Fund for the Integration of Industrialization and Informatization (Information Fusion Methods For Condition Monitoring and Fault Diagnosis of The Marine Electric Propulsion System) under Grant U1709215, in part by the Fundamental Research Funds for the Central Universities of China under Grant 2019-YB-023, in part by the Guangxi Middle-Aged and Young Teachers in Universities of Basic Ability to Improve Scientific Research Project under Grant 2019KY0216, and in part by the China Scholarship Council.

ABSTRACT A novel convolutional neural network namely the modified CNN-GAP model is proposed for fast fault diagnosis of the DC-DC inverter. This method improves the model structure of the traditional CNN by using a global average pooling layer to replace the fully connected layer of 2∼3 layers. The improved CNN-GAP method mainly contains an input layer, a feature extraction layer, a global average pooling (GAP) layer, and a Softmax output layer. Firstly, the raw 1-D time-series data directly input into the input layer of the established CNN-GAP diagnosis model. The 2-D feature maps are reconstructed in the input layer. Secondly, the representative features are automatically extracted from the 2-D feature maps by using multiple convolutional layers and pooling layers. Thirdly, the dimension transformation and size compression of the output image of the feature extraction layer is completed by the GAP layer. Finally, the fault diagnosis result of the DC-DC inverter is automatically output in the Softmax output layer. The proposed method is used for diagnosing the open-circuit fault of the IGBT in the isolated DC-DC inverter. The proposed method is more accurate and effective than other mainstream intelligent diagnosis methods including the SVM, KNN, DNN, and traditional CNN. The experiment results show that the diagnostic accuracy is up to 99.95%, and the testing time can reduce by more than 15%. The improved CNN-GAP method could greatly reduce the model parameter quantity of the traditional CNN more than 80%, which is more suitable for rapid fault diagnosis in electronic devices.

INDEX TERMS Intelligent fault diagnosis, data-driven, convolutional neural network, global average pooling, 2-D feature image, deep learning, DC-DC inverter, IGBT open-circuit fault.

I. INTRODUCTION

Ships are one of the most important water transportation in the world, and it plays an irreplaceable role in the field of shipping [1], [2]. Nowadays, with the rapid development of the shipping industry, the ecological environment of the ocean has been severely damaged because the large pollution gasses and high carbon emissions from fossil fuel combustion of large ships are excessively discharged into the ocean [1]. In the recent decade years, the whole world is facing a series of intractable problems brought by fossil energy such as environmental pollution, reduced reserves and non-renewable [3], [4], etc. Pure electric propulsion ships are the emerging green ships, which have the advantages

The associate editor coordinating the review of this manuscript and approving it for publication was Mingjun Dai.

of energy-saving, environmental protection and ''zero emission'', and have gradually become a key development direction of the most maritime powers [1]. Electric propulsion ships can be powered by wind, solar, fuel cells and ultracapacitors [5]. Due to the variety of power sources and the need to achieve cross networking and energy conversion, the DC-DC inverter plays an extremely important role in the electrical grid system of the electric propulsion ships [1], [6]. To meet the safety standards of an electric power system and flexibility of the system reconfiguration, electrical isolation is often required. The isolated bi-directional DC-DC inverters have become a key component in the electrical power systems of the new hybrid power ship [7]. In the electric propulsion system, the fault and anomaly of the DC-DC inverters will generate an enormous impact on the performance of the power system [6], [7]. In practical applications, the DC-DC inverter needs to run for a long time under complex and changeable operating conditions, which needs to withstand multiple work environments such as over-voltage, over-current, overheating, high and low temperature, corrosion and dust, etc. Therefore, the DC-DC inverters often generate various faults [8]. In general, different from mechanical faults, the initial characteristics of the electrical faults are not very obvious and their upgrade speed is very fast. Once the inverter fails, if it is not timely handled, it will cause fluctuations or imbalances of the power system, the collapse of the entire power grid, and even personal injury. Therefore, it is necessary to establish an intelligent, fast, and automatic fault diagnosis and anomaly detection system to ensure the safe and stable operation of the DC-DC inverter [9]–[11].

According to the relevant studies, most DC-DC inverter failures are caused by the damage of power thyristor in the main circuit of the marine power system, especially the high-frequency Insulated Gate Bipolar Translator (IGBT) in the inverter circuit, accounting for about 38% of all faults [11], [12]. The IGBTs usually run in the high-frequency state with large wastage and heat radiation, and are more likely to fail. The main fault type includes the short-circuit fault (SCF) and open-circuit fault (OCF) [11], [13]. In practice, the short-circuit faults often accompany instantaneous destructive large current. For the SCF, on the power grid system, inverters are usually equipped with over-current detection devices. Once over-current occurs, the power system will be automatically cut off in microseconds. Therefore, there are mature hardware solutions to diagnose the short-circuit faults of the IGBT [14]. Comparing with the SCF, the open-circuit fault is more difficult to detect because the power system can continue to work when the OCF occurs [8]. The main reason is the external performance and fault feature of the IGBT is not obvious when the incipient OCF occurs [14]. Generally, the minimum fault level of the OCF is when only one IGBT is failure. If the minimum fault level of the OCF is not handled timely, it will quickly affect other IGBTs to produce over-current, leading to the rapid evolution and upgrade from the minor fault to significant fault [14]. Actually, the micro fault feature of the minimum fault level of the OCF is difficult to be detected because it is difficult to activate the protection program of the power system [8]. What's worse, the fault upgrade speed of the power device is very fast, which will cause a chain reaction and eventually affect the normal operation of the entire power system. Therefore, the rapid diagnosis and positioning of the incipient OCF of the IGBT in the DC-DC inverters are extremely necessary.

At present, in the electrical DC-DC inverter fault diagnosis field, the mainstream diagnosis approaches include fault mechanism mathematical model-based method [15], [16], expert system knowledge-based method [17], and data driven-based method [18], [19]. The above methods have been applied to some extent, and they have achieved positive and considerable effects on some diagnosis problems. However, some shortcomings of these methods still exist [20], [21]. Model-based diagnosis methods need to establish a high-precision mathematical model that describes the fault evolution mechanisms. This method can obtain better results to some extent. However, establishing a high-precision complex multi-variable system fault model is very difficult. In addition, the established fault mathematical model usually aims to solve specific devices and fault problems, which is difficult to transplant to solve other devices and similar problems [20]. Furthermore, with the increase of the complexity of mechanical and electrical equipment, the mathematical model-based fault diagnosis methods are restricted in practical applications. The expert system-based diagnosis method needs not to establish a high-accurate mathematical model. However, it needs to establish a relatively comprehensive knowledge base, rule base, and inference machine for fault diagnosis [17]. Similarly, these works are very complex and time-consuming. The expert system-based diagnosis method relies excessively on the empirical knowledge of the experts, and the accuracy of diagnosis depends on the considerable amount of expert knowledge in the knowledge base [8]. Furthermore, the knowledge-based fault diagnosis method lacks the ability to autonomic learning, and it is difficult to detect minor or unknown new faults effectively [21]. Nowadays, with the rapid development of ''Internet+'' and industrial big data, the data-driven-based fault diagnosis method has been gradually widely applied to the electronic and electrical equipment such as the voltage detection method [9], current detection method [14], and wavelet transform-based method [25], etc. Although these methods obtain much outstanding effectiveness on some diagnosis problems, these methods still need abundant engineering experiences. It requires engineers to master various advanced signal processing techniques for data preprocessing and feature extraction [20]. Actually, these signal processing techniques and feature extraction methods are difficult to master and a high threshold. These operations are very complex and time-consuming. What's more, different signal types, different fault problem and different diagnosis objections need different signal processing to extract different fault features. Furthermore, the extracted features are mainly used to solve specific fault problems, and its versatility is poor.

In recent years, with the rise of machine learning and deep learning research, intelligence algorithm-based fault diagnosis methods have gradually become a research hotspot [22], [23]. The mainstream intelligent diagnosis method includes the support vector machine (SVM) [18], artificial neural network (ANN) [19], K-nearest neighbor (KNN) [20], and extreme learning machine [22], etc. Through many application and verification, the above three algorithms have poor feature extraction ability due to their shallow network structure, and it is difficult to mine deeply the micro fault features hidden in the monitoring data [20], [23]. Therefore, it is difficult to further improve the fault diagnosis accuracy of these methods. To solve this problem, some scholars usually combine manual feature extraction with shallow machine learning algorithms to perform fault diagnosis [18]–[20]. In these methods, the main fault feature is manually extracted from the raw fault data firstly. Then the extracted features are input into the shallow machine learning algorithm to finish the final fault classification [18]–[20]. In general, the feature extraction methods mainly include Fourier transform (FFT) [18], empirical mode decomposition (EMD) [24], and wavelet transform (WT) [25], etc. Although this combined method can improve the effect of fault diagnosis to some extent, manual feature extraction still needs to rely on the abundant experiences and professional knowledge of the engineers. Additionally, the manual feature extraction operations are very subjective, blind and time-consuming [20]. What's more, many micro-features reflecting the early-time micro-faults are easily deleted as noise, which is very disadvantageous to the rapid and high-effective intelligent diagnosis of the micro fault in mechanical and electrical equipment. Therefore, it is very necessary to explore a more powerful deep machine learning method to mine and extract the deep features of the micro fault.

Fortunately, Hinton and Salakhutdinov [26] propose a novel machine learning method called Deep Learning (DL) in 2006. Deep learning is a great breakthrough in the last decade in the artificial intelligence (AI) field. Different from the traditional shallow machine learning algorithms, the deep learning uses the deep network architectures which can automatically extract the useful representative features from the raw monitoring data layer by layer [20]. At present, it has been successfully applied in many fields such as image recognition, speech recognition, and natural language processing [23]. The convolutional neural network (CNN) is one of the most important branches of deep learning. Compared with other deep learning methods, CNN has more powerful feature extraction capabilities and the potential to overcome the aforementioned inherent shortcomings of the traditional intelligent diagnostic methods on the micro-fault [20]. Since 2013, deep learning has attracted the attention of researchers in the fault diagnosis filed [20], [23]. Literature [23] proposes an intelligent diagnosis method based on a four-layer deep belief network (DBN) to diagnose a closed-loop single-ended primary inductance converter. Literature [25] proposes a novel method by combining the DBN and wavelet packet energy spectrum to diagnose the fault of the converter. Wang *et al.* [27] proposed a motor fault diagnosis method based on short-time FFT and CNN. Although the above studies using deep learning algorithms, they still need some traditional feature extraction methods to extract the features from raw fault data. In their researches, the powerful feature extraction ability of CNN is not only underutilized but also limits the further improvement of the diagnostic effect. Literature [28] proposed a convolutional discriminative feature learning method for the induction motor fault diagnosis by using raw data directly. Although this method improves the shortcoming of the traditional feature extraction in Literature [25], [27], a shortcoming still existed in their research. In their CNN algorithm, the fully connected multilayer perceptron (MLP) was adopted, which lead to the trainable parameter quantity of the fully connected (FC) layer in the CNN model too large. The parameter quantity of the fully connected layer accounts for 80–90% of the total parameter quantity of the CNN model [29]. Actually, a huge parameter quantity will increase the training time and testing time of the CNN diagnosis model. This shortcoming is very disadvantageous to quickly diagnose and the real-time detect the micro-faults of the electrical power inverter.

To solve the abovementioned shortcomings, this paper presents a novel data-driven intelligent fault diagnosis method based on a modified convolutional neural network with a global average pooling layer and 2-D feature image for fast fault diagnosis of the DC-DC inverter. The main contributions of this paper are summarized as follows. Firstly, a novel fast fault diagnosis frame based on improved CNN-GAP is proposed. The proposed method improves the traditional CNN algorithm structure by using a global average pooling (GAP) layer to replace the fully connected layer with a 2∼3 layer. The proposed CNN-GAP algorithm contains an input layer, a feature extraction layer, a GAP layer, and a Softmax output layer. Secondly, the improved method can effectively reduce the model trainable parameters quantity and diagnosis waiting time of the traditional CNN model, which is more suitable for rapid fault diagnosis and real-time anomaly detection in electronic devices. Thirdly, the proposed method need not any manual feature extraction and feature selection method on raw 1D time-series signals data. The raw voltage signals data directly input into the input layer of the improved CNN-GAP model. The raw 1-D time-series is automatic data reconstructed into 2-D feature maps in the input layer. Then, the representative features are automatically extracted from the 2-D feature maps by the feature extraction layer. The dimension transformation and size compression of the output image of the feature extraction layer is completed by the GAP layer. The fault diagnosis result of the DC-DC inverter is automatically output in the Softmax output layer. The proposed method can greatly get rid of the dependence on expert knowledge and engineering experience. The experiment result confirms the proposed method is more effective than other existing mainstream intelligent diagnosis methods

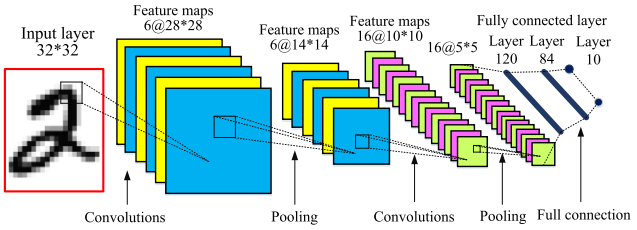

FIGURE 1. The basic structure of the convolutional neural network.

including SVM, KNN, ANN, DNN, and traditional CNN. The end-to-end algorithm structure of the proposed method has better operability and versatility.

The rest of this paper is organized as follows. In section 2, the basic theory of CNN is given briefly. In section 3, the improved CNN-GAP model structure and approach is described in detail. In section 4, the proposed method is applied to diagnose the open-circuit fault signals of the IGBT in the DC-DC inverter, and experimental results are analyzed and discussed. Finally, the conclusions and future works are given in section 5.

II. CONVOLUTIONAL NEURAL NETWORK PRINCIPLE

The convolutional neural network (CNN, also known as ConvNets) is one of the most important branches of deep learning technology [20], which is a special deep-layer structure of the feed-forward artificial neural network (ANN) [27]. It was first proposed by Yann LeCun [23] in 1989 and is mainly used for handwritten figure recognition. The CNN is inspired by the layered structure of the animal's brain, and the animal vision system working principle is simulated in the CNN model. Different from the traditional fully connected ANN, the CNN has three outstanding advantages: firstly, the CNN has the powerful feature extraction ability by constructing multiple filters (also known as convolution kernels or neuron) and using these filters to automatically extract the representative features from the input data layer by layer [20]. Secondly, CNN can greatly reduce the number of training parameters by combining the sparse connection with the parameter weight sharing mechanism [30]. Each convolution kernel is only sparsely connected to a small region of the feature map in the previous layer on the CNN [31], [32]. The data dimension is down-sampled in time and space, which effectively avoids over-fitting of the model. Thirdly, CNN has a good adaptive ability to scaling, tilting, and translation of the images. Nowadays, CNN is great widely applied in image recognition and other similar problems [20]. In general, CNN has many different model structures. A classical LeNet-5 CNN structure is shown in Figure 1 [31]. In Figure 1, this is a multi-stage neural network that consists of several filter stages and one classification stage. The filter stage is used to extract representation features from the input data, which contains two kinds of layers: the convolutional layer and the pooling layer. The classification stage is a multi-layer perceptron fully connected network, which is composed of several fully-connected layers and a Softmax classifier. The basic components of the CNN algorithm are introduced as follows.

A. CONVOLUTIONAL LAYER

The convolutional layer is one of the most important core modules on CNN. The main role of the convolutional layer is to extract the representation feature from the input image by several convolutional kernels (also known as filter or neuron) [30]. In general, each filter will extract a type feature. Different filters will extract different features. In order to extract more features, the more convolutional kernel is used in the convolutional layer [20]. During the forward propagation process, each filter is used to convolve with the input feature map. Through the convolutional calculation, many new feature maps are generated and as the input of the next layer. The mathematical expression [33] of the convolution operation can be described as follows:

$$X_i^{(k)} = f\left(\sum_{c=1}^{C} W_i^{(c,k)} \otimes X_{i-1}^{(c)} + B_i^{(k)}\right) \tag{1}$$

where $\otimes$ represents the convolutional operator; i denotes the index of the network layer; k represents the index number of the convolution layer output feature maps and also marks the k th group convolution kernel; each group contains C convolution kernel; $k = 1, 2, \ldots,$ K; $c = 1, 2, \ldots,$ C and is the channel index number of input feature maps; $X_{i-1}^{(c)}$ is the input feature map of channel c; $X_i^{(k)}$ is the kth output feature map after the convolution calculation of the kth group convolution kernel and the input feature map; $W_i^{(c,k)}$ is the weight of the convolution kernel at the ith layer, the filter of cth channel in the kth group convolution kernel; and $B_i^{(k)}$ is the bias of the kth group filter in the ith layer. In this paper, because the monitoring signal of the DC-DC inverter is a voltage signal, therefore, C=1; $f(\cdot)$ is the nonlinearity activation function. In the CNN, the most common activation functions include the Sigmoid, hyperbolic Tangent, and Rectified linear unit (RELU). Different activation functions can obtain different nonlinear transformations. In this paper, the RELU function is used as the activation function of the proposed method because it can more effectively reduce the gradient disappearance and over-fitting of the CNN model [20].

B. POOLING LAYER

The pooling layer (also known as sub-sampling layer or down-sampling layer) is commonly applied after the convolution layer in the CNN architecture. The main role of the pooling layer is to down-sampling the feature dimensions and to compress the size of the received feature map. Pooling operations mainly include maximum pooling and average pooling [30]. In CNN, the most common pooling layer is the max-pooling [33]. The mathematical expression of the max-pooling can be described as follows [20]:

$$P_i^{(k)} = \max_{\substack{(j-1)S+1<t_x\le jS \\ (j-1)H+1<t_y\le jH}} \left\{X_i^{(k)}\left(t_{x,y}\right)\right\} \tag{2}$$

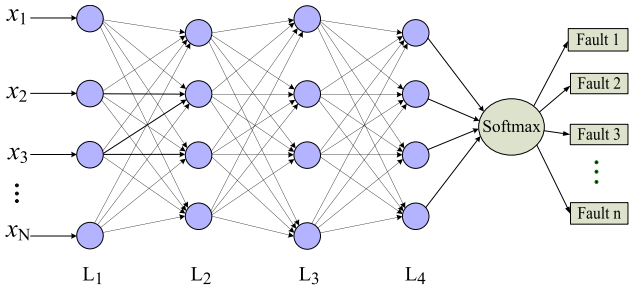

FIGURE 2. The schematic diagram of the fully connected network.

where $X_i^{(k)}\left(t_{x,y}\right)$ represents the $t_{x,y}$th pixel value in the kth output feature map of the ith layer, S and H are the width and height of the pooling window respectively, $\left\{X_i^{(k)}\left(t_{x,y}\right)\right\}$ is a matrix of the shape $S \times H$, and is the output feature map after the pooling operation. In this paper, the max-pooling is applied in each pooling layer. The size of the pooling kernel is 2×2, and the stride size is 2. So, each feature map after the pooling operation will reduce 75% parameter quantity [20].

C. FULLY CONNECTED LAYER

After alternately stacking multiple convolutional layers and pooling layers, the fully connected (FC) layers are followed to calculate the class scores [27]. The detailed process is shown in Figure 2. In the traditional CNN, the fully connected layers commonly contain 2∼3 layers fully connected multilayer perceptron.

Usually, the final output feature map of the CNN is transformed into a one-dimensional array by a Flatten layer [28]. Then, the 1-D array is as the input layer of the FC layer. Finally, the output of the FC layer has n neuron. The n neuron represents n fault types. In the fully connected network, all neurons between layers are interconnected, with the following definition [20]:

$$o(X) = f(W \cdot X + B) \tag{3}$$

where $f(\cdot)$ denotes the activation function; X is the input of the fully connected layer; $o(X)$ is the output of the fully connected layer; W and B are the weights and biases of a fully connected network, respectively.

By summarizing the existing literature of the CNN model, in the traditional CNN, the main role of the fully connected layer contains two aspects [27]–[33]. On the one hand, the FC layers are used to further extract the representative features from the output feature maps of the last pooling layer on the CNN. On the other hand, the fully connected layer acts as a transitional bridge to connect the last pooling layer of CNN to the Softmax classifier. However, in actual, there have some inherent shortcomings in the fully connected layer. Firstly, the FC layer has too many trainable parameters. The parameter quantity of the FC layer accounts for 80–90% of the total parameter quantity of the CNN model [29]. Moreover, the number of parameters increases exponentially with the increasing number of the FC layers [20]. Secondly, in the traditional CNN, the FC layer is not only occupied too much computing resources but also easily leads to the CNN model over-fitting and gradient disappeared [29]. Thirdly, the FC layer resulting in the training time and testing time of the traditional CNN is too long. This shortcoming will lead to the trained fully connected CNN model not suitable for rapid fault diagnosis and real-time anomaly detection in the electronic DC-DC inverter.

III. PROPOSED CNN-GAP INTELLIGENT DIAGNOSIS METHOD

To solve the abovementioned shortcomings of the traditional CNN model and the mainstream shallow machine learning algorithms, in this paper, it develops a novel data-driven intelligent fault diagnosis method based on the modified convolutional neural network with a global average pooling layer and 2-D feature image for fast fault diagnosis of the DC-DC inverter. The proposed CNN-GAP algorithm contains an input layer, a feature extraction layer, a global average pooling layer, and a Softmax output layer. The proposed arithmetic structure in detail is shown in Figure 3. Different from the traditional CNN, the proposed method improves the traditional CNN algorithm structure, by using a global average pooling layer to replace the fully connected layer with 2∼3 layers. The proposed method designs a global average pooling layer behind the feature extraction layer. Compared with the traditional CNN model, the improved CNN-GAP model is better than the traditional CNN model with the fully connected layer. The main advantages of the modified CNN-GAP can be summarized as follows: firstly, the improved CNN-GAP has less trainable parameter quantity. The GAP layer could greatly reduce the training parameters quantity of the traditional CNN model. In our experiment, the improved CNN-GAP could effectively reduce the parameter quantity of more than 80%. Secondly, the improved CNN-GAP method has more fast diagnosis speed and more few testing times of fault diagnosis. The proposed method reduces the model layer quantities and model complexity of the traditional CNN model by removing the fully connected layer. Therefore, the trained CNN-GAP model has fewer testing waiting times. It is very suitable for rapid fault diagnosis and real-time anomaly detection in electronic devices. Thirdly, the improved CNN-GAP method could further reduce the risk of model over-fitting and avoid the gradient disappearance problem by reducing the number of network layers and trainable parameter quantity of the original CNN model. The proposed method need not any manual feature extraction and feature selection operations on the raw signals data. It can greatly get rid of the dependence on expert knowledge and engineering experience. The end-to-end model structure of the proposed method has better operability and versatility.

In the proposed method, the main working principle is as follows: firstly, the raw one-dimensional time series fault data can directly input into the improved CNN-GAP model without any manual feature operation. The input layer could

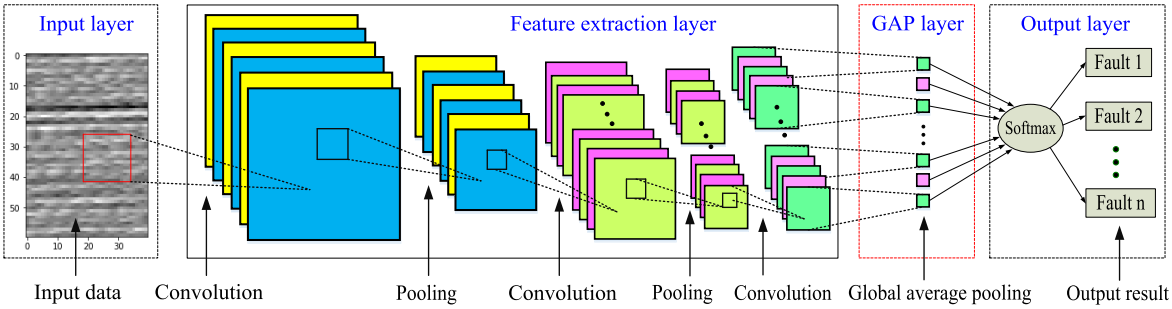

FIGURE 3. The model structure of the improved CNN-GAP method.

automatically transform the 1-D time-series input data into 2-D feature maps by a data reconstruction method. Secondly, the feature extraction layer could automatically extract the useful representative features from 2-D input feature maps layer by layer. Thirdly, the dimension transformation and size compression of the output feature map of the feature extraction layer is completed by using the global average pooling layer. Finally, the output of the GAP layer is fed into the Softmax output layer. The fault diagnosis result of the DC-DC inverter is automatically output in the Softmax output layer. In our method, the output feature map channel (dimension) quantity of the last convolutional layer in the feature extraction layer should be set to the same as the number of the fault categories. Here, it is assumed that there are n fault categories. By the GAP layer operation, each output feature map of the feature extraction layer will be transformed into one value. So, the output of the GAP layer is a 1-D array which has n value. The basic flow chart of the improved CNN-GAP intelligent fault diagnosis algorithm is shown in Figure 4.

In Figure 4, the proposed method is used for diagnosing the micro-fault of the DC-DC inverter. The main procedure of the proposed method for fault diagnosis can be summarized as follow:

Firstly, the raw fault monitoring signal data of the diagnostic object are obtained by various sensors such as voltage signal, and electric current signal, etc.

Secondly, some data process operations are applied in the input layer such as data normalization, data segmentation, data reconstruction, and data augmentation, etc. Through these data process operations, the fault samples and fault datasets are established for the training and testing of the CNN-GAP diagnosis model.

Thirdly, all the samples of each fault type after the data process are randomly divided into a training dataset, a validation dataset, and a testing dataset. The training dataset is used for training the CNN-GAP model. The verification dataset is used for verifying the accuracy of the trained CNN-GAP model. The testing dataset is used for the final fault classification and accuracy assessment of the trained CNN-GAP model.

Fourthly, the improved CNN-GAP fault diagnosis model is adjusted. Initialize the CNN-GAP model parameters. The established CNN-GAP model is trained by multiple epoch

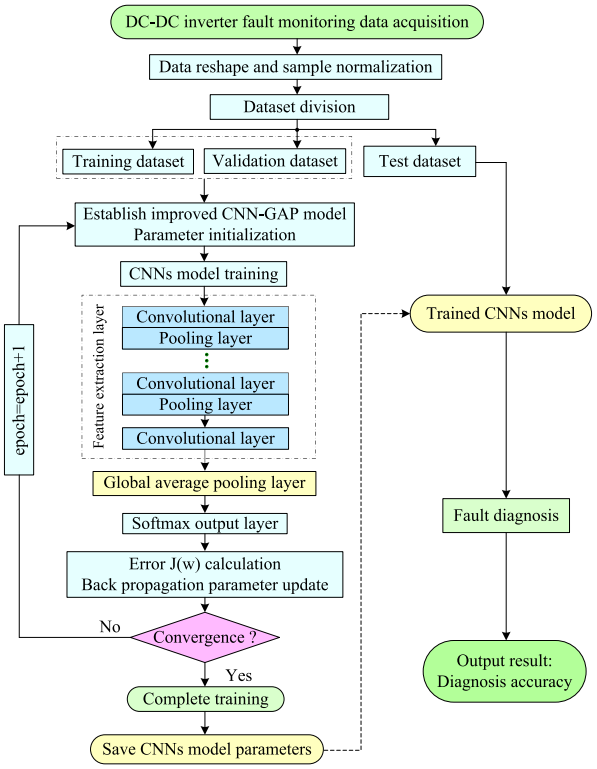

FIGURE 4. The flow chart of the CNN-GAP intelligent diagnosis algorithm.

repeated iterative calculations. In this section, the fault samples of the training dataset are fed into the established CNN-GAP model. In the training stage, the forward propagation and the back-propagation are performed in each iteration calculation. The error between the forward-propagation predicted result of the CNN-GAP model and the actual label of the sample is calculated. The loss function $J(w)$ is minimized by the error back-propagation algorithm. During the training process, the verification dataset is used for verifying the accuracy of the trained CNN model. After several iterations of the CNN-GAP model, when the accuracy rate on the verification dataset is obviously lower than the accuracy rate on the training dataset, it indicates that the CNN-GAP model may generate the over-fitting. Here, the model training should be stopped timely. Through repeated to adjust parameter and testing, the model hyper-parameter is compared and selected according to the precision curve of the verification set.

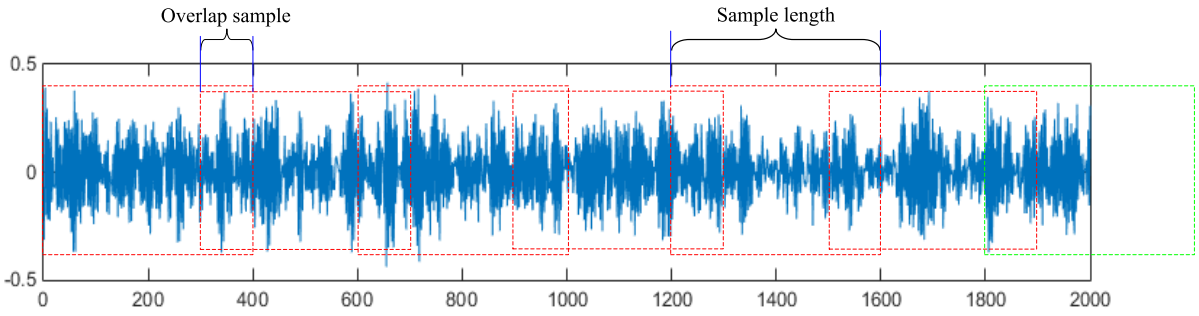

FIGURE 5. The data segmentation of the overlap sampling method.

The training process of the CNN-GAP model is finished when the accuracy rate of the verification dataset meets the requirement.

Finally, the testing dataset data is input into the trained CNN-GAP model, the representative feature of the raw input data is automatically extracted by using the trained CNN-GAP model. The final classification result of fault diagnosis is automatically outputted.

In the proposed method, the basic components of the improved CNN-GAP algorithm are as follows.

A. INPUT LAYER

In the proposed CNN-GAP model, the main role of the input layer contains two aspects. The one is to receive the raw 1-D time-series fault date from the monitoring sensors. The other is to make some necessary data process operations that could transform the raw 1-D data into the standard formation to meet the input data format requirements of the CNN-GAP model. The common data process operations mainly include data normalization, data segmentation, data format reconstruction, data augmentation, etc [32], [33].

1) DATA NORMALIZATION

In general, different fault types will obtain different raw fault monitoring data. These data usually is a continuous and long-time 1-D time-series data. Different fault monitoring raw data have different magnitudes and amplitudes range under the data acquisition process in actual. However, the large magnitude difference between the different fault samples is disadvantageous to train the CNN model [20]. To solve this problem, data normalization is a common and effective method. Each fault monitoring raw data is normalized into the range [0, 1] in advance. The common data normalization is the mean value method [34], and the mathematical expression [20] is described as follows:

$$X = \{x_i\} = \frac{x_i - x_{\min}}{x_{\max} - x_{\min}} \tag{4}$$

where $x_{\max}$ represents the maximum value in the input sample, $x_{\min}$ represents the minimum value in the sample, X is the result after standardization, and the value range is between 0 and 1.

2) DATA SEGMENTATION

After the data normalization, each fault sample data still is a long 1-D time-series data. In the CNN model training process, if this long 1-D time-series data are inputted into the CNN model one-time, it will not be processed due to the computer memory overflow. To solve this problem, the data segmentation [20] is adopted. According to the sampling period, the fault occurs frequency or other references, the long 1-D time-series data can be segmented as many equal length short 1-D time-series data segments. Here, each short 1-D time-series data segment is a fault sample. To improve the correlation between adjacent samples, in this paper, the overlap sampling method is designed by using a sliding window [33]. Through this method, it can obtain more fault samples for training and testing of the CNN-GAP diagnosis model, as shown in Figure 5.

In Figure 5, this long 1-D time-series data segment has 2000 data points. Through data segmentation, it obtains 6 samples by using a sliding window overlap sampling method. The length of each new sample is 400 points. The data point quantity of the overlapping sample is 100 points (the overlapping radio is 25%). The sample quantity calculation method of the overlap sampling can be defined as follows:

$$Sample_{num} = \frac{input_{length} - Window_{length} + 1}{stride_{length}} \tag{5}$$

where $input_{length}$ represents the data point quantity of the raw long 1-D time-series data segment, $Window_{length}$ represents the data point quantity of the sliding window, $stride_{length}$ represents the data point quantity of each stride. $Sample_{num}$ is the new fault sample quantity by using the overlap sampling method. It should be noted that the decimal point of the calculation result should be treated as an integer. For instance, in Figure 5, the $input_{length}$ is 2000, the $Window_{length}$ is 400, the $stride_{length}$ is 300, therefore, $Sample_{num}$ is 6. It can be seen from Figure 5, the rightmost sample is incomplete, so it can not be used as a sample.

3) DATA RECONSTRUCTION

In general, CNN is widely used for processing the data with mesh-like structures [20]. The input data format of CNN is

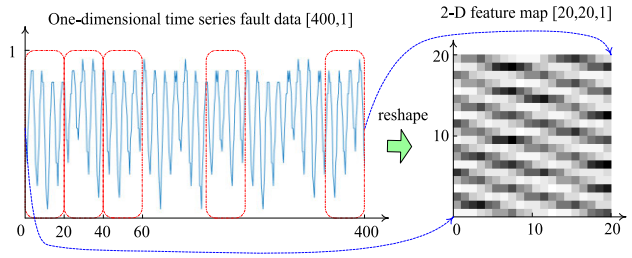

FIGURE 6. The procedure of data reconstruction from 1D transform to 2D.

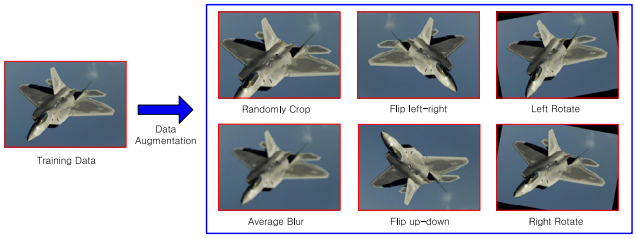

FIGURE 7. The schematic diagram of the data augmentation operation.

usually 2-D image data or 3-D video data [30]. After the data segmentation, each fault sample is still a short 1-D time-series. To meet the input data format requirement of CNN, in this paper, each short 1-D time-series data can be transformed into a 2-D feature map format by using the data reconstruction method [20]. The data reshaping process is shown in Figure 6.

4) DATA AUGMENTATION

To improve the generalization ability and robustness of the trained CNN model, in the input layer of the proposed CNN-GAP method, the data augmentation [35] is applied. The data augmentation is a good approach to expend the sample quantity of the raw fault dataset by a series of small-scale random image transformations [20]. It has been widely used in image recognition [36]. The common data augmentation operations include random cropping, rotation, flipping, etc. The demonstration of the data augmentation operations is shown in Figure 7. In Figure 7, the left side is the raw feature map. The right side is six data augmentation operations including the random cropping, left-right flipping, left rotation, average blurring, up-down flipping, and right rotation of the original data. As can be seen from Figure 7, an aircraft is still an aircraft after six data augmentation operations.

B. FEATURE EXTRACTION LAYER

The feature extraction layer is an important part of the improved CNN-GAP method. The main function of the feature extraction layer is to extract the deep representative feature from the 2-D input feature map fault data. The feature extraction layer is similar to the traditional CNN which composed of several convolutional layers and pooling layers. A deep feature extraction layer could be constructed by alternately stacking multiple convolution layers and pooling layers. In general, the deep feature extraction layer can extract more deep representative features. However, with the increase of the layer quantity, the gradient disappearance may have occurred in the training process of the CNN model. So, it needs to design a suitable CNN model structure according to the actual needs of the diagnostic object. A detailed description of the convolutional layer and pooling layer can refer to Sections 2.1–2.2.

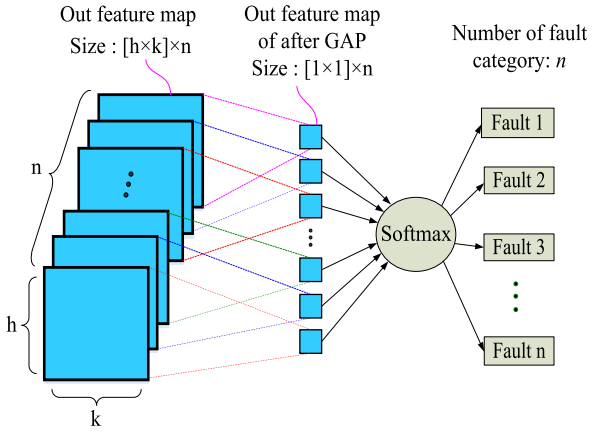

FIGURE 8. The structure of the GAP operation of the CNN-GAP method.

C. GLOBAL AVERAGE POOLING LAYER

The global average pooling (GAP) layer is a core section of the improved CNN-GAP method. The global average pooling is a new technique to solve the problem of too many model parameters of the fully connected network in the traditional CNN [29]. The main principle of the GAP is similar to the max-pooling operation of traditional CNN. However, different from the ordinary max-pooling operating, multiple special global average pooling filters (also known as pooling window) are used in the GAP layer [20]. The GAP filter is a special rectangular matrix. A detailed structural design of the GAP is shown in Figure 8.

In Figure 8, it assumes that the size of each output feature map before the GAP operation is h×k, by using the GAP filter, the output of the GAP is 1 × 1. The main process of the GAP operation can be summarized as follows: firstly, the several global average pooling filters are designed. The number of the GAP filter is set to the same as the number of the output feature map. Assuming that the number of output feature map is n, the number of the GAP filter is set as n. Secondly, the size of each GAP filter is set to the same as the size of the output feature map. So, the size of the GAP filter is set as h×k. Then, each GAP filter calculates a global average value from the corresponding each output feature map. Finally, the size of the output feature map after the GAP operating is 1 × 1. The mathematical expression [20] of the GAP operation can be rewritten as Formula 6.

$$S^{l}_{avg-pooling} = \frac{1}{c}\sum_{i=1}^{c} X^{l}_{1:h,1:k,i} \tag{6}$$

where $S^{l}_{avg-pooling}$ represents the calculated result by the global average pooling of the l-th output feature map; l is the index of output feature maps; c represents the total number of element values in the global average pooling kernel; 1: h denotes that the range of a pooling kernel in the height

direction is from the 1st line to the h-th line; 1: k indicates that the range of a pooling kernel in the width direction is from 1st column to the k-th column; similarly, the h and k respectively represent the height and width of an output feature map; and $X^{l}_{1:h,1:k,\ i}$ represents the element value corresponding to the global average pooling filter.

Here, it is assumed that there are n fault classification categories. By the GAP operation, each output feature map will be converted into one value. So, the output of the GAP layer is a 1-D array which has n value. Then, the output of the GAP layer is fed into the Softmax output layer. Finally, the results of classification and diagnosis could be automatically output by the Softmax layer. It can be seen from Figure 8, the input of the Softmax classifier is a 1-D array which has n value. Therefore, in this method, the output feature map channels (dimensions) quantity of the last convolutional layer in the feature extraction layer should be set to the same as the number of the fault categories. Through these designs, it realizes a perfect connection and transition between the output of the feature extraction layer and the input of the Softmax classifier. The forward-propagation and error back-propagation can be performed in the improved CNN-GAP method. In this method, the GAP layer has not any training parameters. The global average pooling technique could greatly reduce the training parameters quantity and model complexity of the traditional CNN model by removing the 2∼3 layers fully connected network. Therefore, the improved CNN-GAP method could further reduce the risk of the model over-fitting and more suitable for rapid fault diagnosis and real-time anomaly detection in electronic devices.

D. SOFTMAX OUTPUT LAYER

Softmax is the most commonly used classification function in pattern recognition [27]. In the proposed CNN-GAP method, the main role of the Softmax layer is to convert the output result of the GAP layer to a new final result which meets a probability distribution [20]. Usually, the output result of a fully connected layer is a 1-D array [33]. This 1-D array has n quantized value. Actually, the n quantized value has different magnitudes that do not conform to the probability distribution. To solve this problem, the Softmax function is used for normalizing the calculation. After the Softmax normalization, the output of the Softmax layer is a 1-D vector that conforms to the probability distribution [20]. Each value is converted to a value between 0 and 1, and the sum is 1. Assuming that the training input sample is x and the corresponding label is $\bar{y}$, sample x is predicted to be the probability of category j, which can be defined as $P(y = j \mid x)$. The Softmax function mathematical expression can be defined as [27]:

$$Y_i^{'} = \begin{bmatrix} P(y_i = 1 \mid x_i) \\ P(y_i = 2 \mid x_i) \\ \vdots \\ P(y_i = n \mid x_i) \end{bmatrix}^T = soft\max(Y_i) = \frac{1}{\sum_{l=1}^{n} e^{x_i^T \cdot w_l}} \begin{bmatrix} e^{x_i^T \cdot w_1} \\ e^{x_i^T \cdot w_2} \\ \vdots \\ e^{x_i^T \cdot w_n} \end{bmatrix}^T \quad (7)$$

where $Y_i^{'}$ is the output value of the ith sample after normalization by Softmax; $Y_i^{'} = (y_i^{(1)'}, \cdots, y_i^{(l)'}, \cdots, y_i^{(n)'})$; the range of each value of $Y_i^{'}$ is from 0 to 1, and $\sum_{l=1}^{n} y_i^{(l)'} = 1$, conforming to the probability distribution; $P(y_i = 1 \mid x_i)$ is the probability value of the ith sample, belonging to category 1; $e^{x_i^T \cdot w_1}$ represents converting $y_i^{(1)}$ to a value between 0 and 1; $1/\sum_{l=1}^{n} e^{x_i^T \cdot w_l}$ is a normalization function; the maximum value of each row in $Y_i^{'}$ is the fault category predicted of the CNN-GAP model.

The loss error can be calculated by comparing the normalized prediction result with the corresponding sample actual label. In this paper, the cross-entropy loss function is applied. Assuming that the input dataset has m samples, the cross-entropy cost function is defined as follows [20], [37]:

$$J(w) = -\frac{1}{m}[\sum_{i=1}^{m}\sum_{j=1}^{n} I\{\bar{y}_i = j\} \log \frac{e^{x_i^T \cdot w_j}}{\sum_{l=1}^{n} e^{x_i^T \cdot w_l}}] \quad (8)$$

where i represents the ith training sample, j represents the jth category (the total number of categories is n), and $I\{\cdot\}$ is a logical indication function. If the value in the brackets is true, I = 1, else I = 0. $\bar{y}_{(i)}$ is the actual label of the ith sample. $J(w)$ is a cross-entropy loss value. The training process of CNN is to constantly adjust the parameters in Equation 8 to minimize the cost function $J(w)$.

In this paper, the gradient descent algorithm is used for minimizing the loss function $J(w)$ according to the rule of error back-propagation [37]. The weight and bias of the model's trainable parameters are updated in the training process of the CNN-GAP model. In this paper, the Adam [38] optimization algorithm is applied to train the CNN-GAP model. In the Adam algorithm, the learning rate can automatically adjust the learning rate step length according to the local error surface of the mini-batch sample. The basic training process of the Adam adaptive learning rate optimization algorithm [38] can be described as follows:

IV. FAULT DIAGNOSIS FOR THE ISOLATED DC-DC INVERTER

To verify and evaluate the effectiveness and feasibility of the improve CNN-GAP method for the intelligent and fast diagnosis in electronic devices, in this paper, the proposed method is applied to diagnose and identify the open-circuit fault of the IGBT in the isolated three-phase bridge bidirectional DC-DC inverter. In this experiment, the open-circuit fault data of the 12 IGBTs from the isolated DC/DC inverter simulation model are obtained and processed firstly. Secondly, the fault dataset of the IGBT is established. Thirdly, the raw fault data

Adam Adaptive Moment Optimization Algorithm

Require: ε: Stepsize (default setting is 0.001)
Require: ρ_1, $\rho_2 \in [0, 1)$: Exponential decay rates of the Moment estimates. (default setting is 0.9 and 0.999)
Require: δ: Small constant used for numerical stabilization. (default setting is 10^{-8})
Require: θ: Initial training parameters
$t \leftarrow 0$: Initialize time-step
$s_0 \leftarrow 0$: Initialize 1st order moment variable
$r_0 \leftarrow 0$: Initialize 2st order moment variable
While θ_t not converged **do**
Random extracting a mini-batch of m samples $\{x_1, x_2, \cdots, x_m\}$ from the training data set, the corresponding target is $\{y_1, y_2, \cdots, y_m\}$.
$g_t \leftarrow \frac{1}{m}\nabla_\theta \sum_i L(f(x_i; \theta_t), y_i)$: Update gradient
$t \leftarrow t + 1$: Update time step
$s_t \leftarrow \rho_1 \cdot s_{t-1} + (1 - \rho_1) g_t$: Update biased 1st order moment estimate
$r_t \leftarrow \rho_2 \cdot r_{t-1} + (1 - \rho_2) \cdot g_t^2$: Update biased 2st order moment estimate
$\hat{s}_t \leftarrow s_t / (1 - \rho_1^t)$: Compute bias-corrected 1st order moment estimate
$\hat{r}_t \leftarrow r_t / (1 - \rho_2^t)$: Compute bias-corrected 2st order moment estimate
$\Delta\theta = -\varepsilon \cdot \hat{s} / \left(\sqrt{\hat{r}} + \delta\right)$: Calculate the update value
$\theta_t \leftarrow \theta_{t-1} + \Delta\theta$: Update parameters
end while
return θ_t (Resulting parameters)

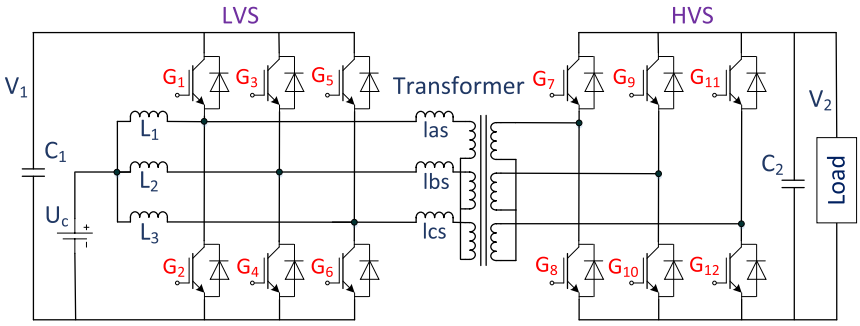

FIGURE 9. The working principle diagram of the isolated three-phase bridge bidirectional DC/DC inverter.

are input into the improved CNN-GAP model without any manual feature extraction. Finally, fault diagnosis results are automatically outputted.

A. THREE-PHASE ACTIVE BRIDGE ZVS BIDIRECTIONAL DC/DC INVERTER

The isolated bidirectional DC/DC inverter is an important functional part of the modern power system. In the electric propulsion ship, it plays an irreplaceable role due to the variety of power sources and the need to achieve cross networking and energy conversion [1], [2]. The isolated bidirectional DC/DC inverter has a high-frequency transformer between the input side and output side. It could be effectively achieved electrical isolation. At present, it has been widely applied in medium and large power conversion occasions [7]. The working principle diagram of the three-phase active bridge ZVS bidirectional DC/DC inverter is shown in Figure 9. In Figure 9, the DC/DC inverter is composed of three single-phase half-bridge DC/DC topologies. The three-phase topology works with 120° interleaving, and the low-voltage side (LVS) half-bridge has two functions: 1) As a boost inverter, which is implemented with a three-phase inductor and an LVS half-bridge; 2) Generating a high-frequency AC voltage [40].

At present, the common monitoring signals mainly include voltage signals and current signals for fault diagnosis of the IGBT open circuit fault in the DC-DC inverter [14]. Because the current signal is susceptible to load changes and fluctuations, in this paper, the output voltage of the DC-DC inverter is used as the monitoring signal of fault diagnosis. Through a lot of research studies, it found when the open-circuit fault of multiple IGBTs occurred at the same time, the power system will generate significant fault conditions, even power interruption. However, when only one IGBT generates open-circuit fault at one-time, the power system still could continue to work in actual [8]. Because the open-circuit fault feature of the single IGBT is not obvious, so the electronic system protector is not easy to activate.

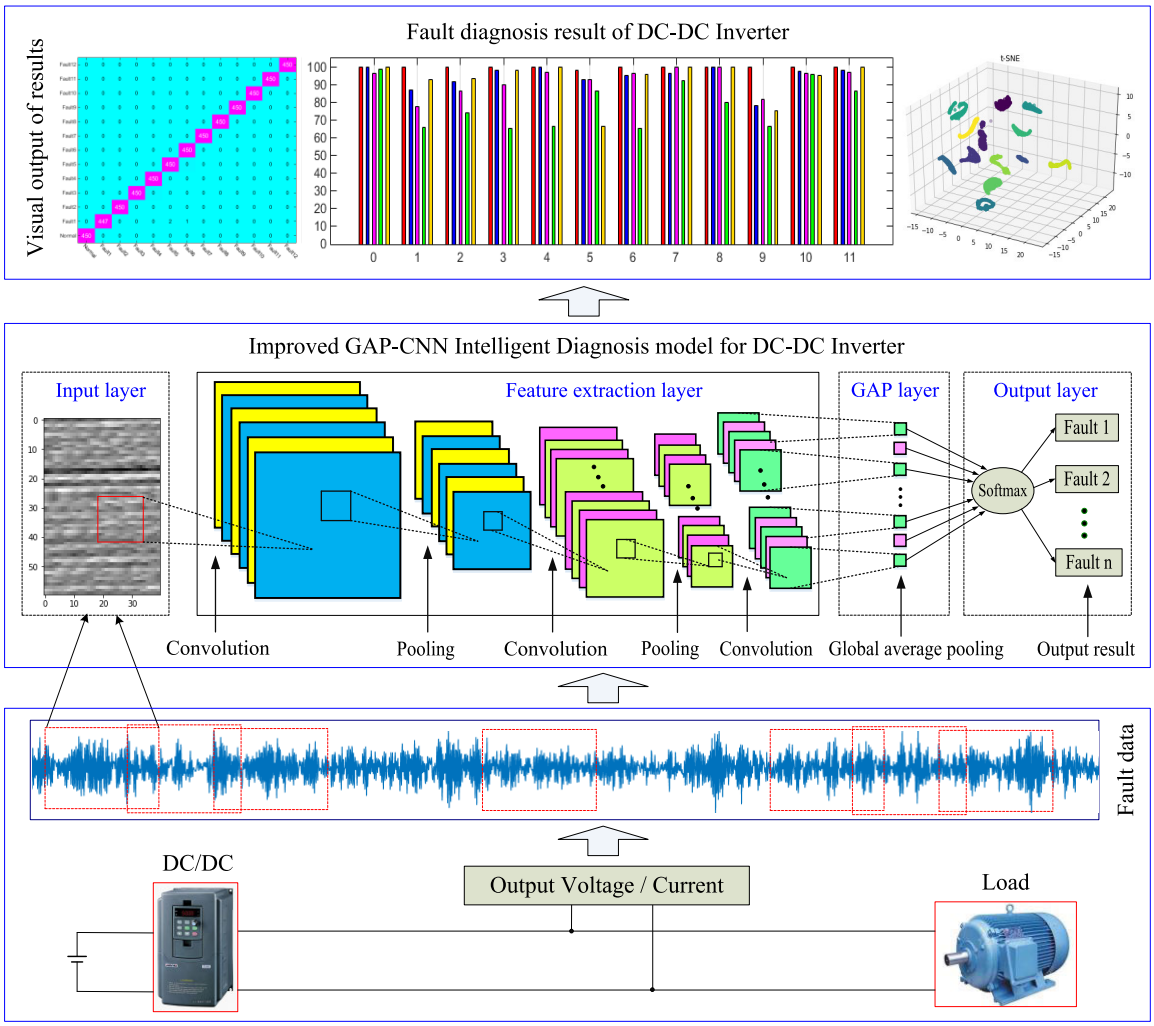

FIGURE 10. The system framework of the improved CNN-GAP intelligent fault diagnosis model.

In general, the open-circuit fault of single IGBT is the minimum fault level. It is easier to ignore because the fault feature is difficult to detect. Therefore, this paper focuses on research the rapid diagnosing and positioning of the incipient open-circuit fault of the IGBT in the DC-DC inverters.

B. INTELLIGENT FAULT DIAGNOSIS FOR THE DC-DC INVERTER BASED ON THE PROPOSED METHOD

According to the aforementioned research result, in this paper, a novel intelligent and fast fault diagnosis frame based on the improved CNN-GAP algorithm is proposed for diagnosing the IGBT open circuit fault in the DC-DC inverter. The framework structure of the proposed fault diagnosis model is shown in Figure 10. In Figure 10, there are three modules. The lowest layer is the fault data acquisition module of the DC-DC inverter. The top layer is the result output module of the fault diagnosis, and the middle layer is the proposed CNN-GAP intelligent algorithm module. In this intelligent diagnosis framework, the common monitoring signal of the DC-DC inverter includes the voltage signal and current signal, etc. The raw 1-D time-series fault data of the DC-DC inverter can directly input into the proposed diagnosis system without any manual feature extraction and signal processing operations. The fault diagnosis result is automatically output in real-time. The proposed method can greatly get rid of the dependence on expert knowledge and working experience. This intelligent diagnosis system is an end-to-end framework structure that has better operability and generality than traditional intelligent diagnosis methods.

In this paper, the isolated three-phase bridge bidirectional DC/DC inverter simulation model is established by MATLAB Simulink software, as shown in Fig. 11. MATLAB Simulink is a superior simulation platform which has realistic simulation performance and has widely applied in the field of electrical equipment development. In this paper, the simulation model is used to investigate all possible combinations of the open-circuit fault of the IGBT. The DC/DC inverter has 12 IGBTs. It supposes that only one IGBT failing at one-time. Therefore, there are 13 health states including 12 fault states and one normal state. In Figure 11, the isolated bidirectional DC/DC inverter model has a single 100V DC source. The primary side and secondary side of the transformer

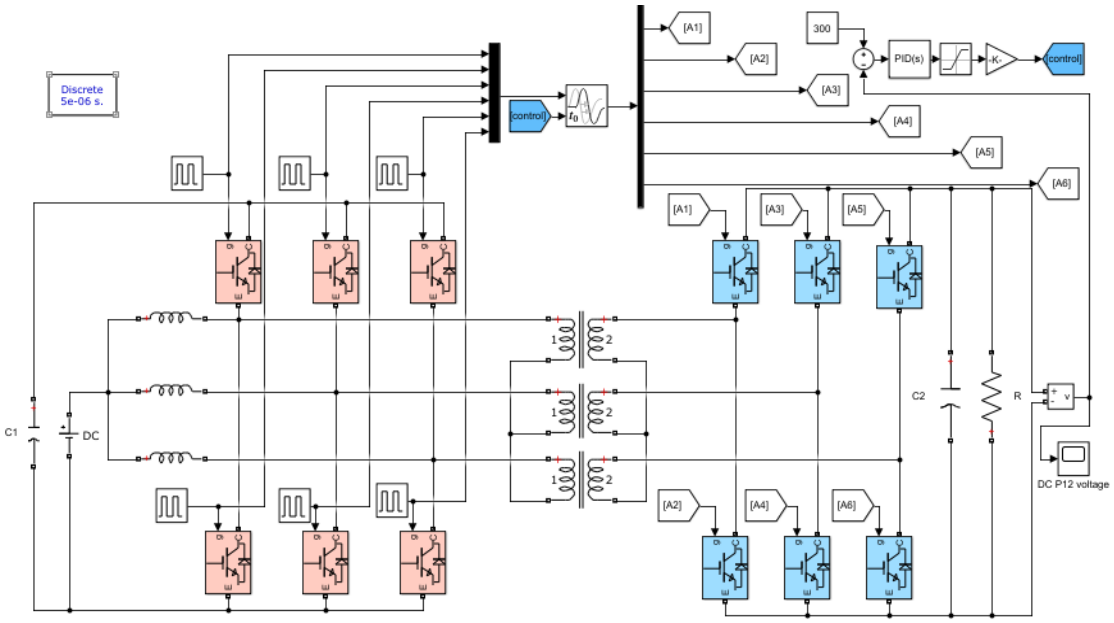

FIGURE 11. Isolated three-phase bridge bidirectional DC/DC inverter simulation model.

TABLE 1. The model parameters of the isolated three-phase bridge bidirectional DC-DC inverter.

Parameters	Value
Switching frequency($1/T_f$)/kHz	20
High voltage winding resistance R_{HVS}/Ω	0.7588
Low voltage winding resistance R_{HVS}/Ω	0.0591
Leakage inductance L_σ/mH	0.232
Excitation impedance R_m/kΩ	100
Magnetizing inductance L_m/mH	456
HVS capacitance C_1 /mF	20
LVS capacitance C_2 /mF	10

consist of six power-switching devices to build full-bridge switching circuitry respectively. The six power-switching devices of the primary side are IGBT G1∼ IGBT G6 respectively. The six power-switching devices of the secondary side are IGBT G7∼ IGBT G12 respectively. The step-up ratio is 1:4 between the primary side and the secondary side. The main parameters of the DC-DC inverter are listed in Table 1.

The fault data are collected from the voltage output interface of the DC-DC inverter simulation model. In this experiment, the sampling frequency is 24 kHz. The sampling time of each fault state is 20 seconds. Therefore, each fault type obtains a long 1-D time-series data segment which has 480,000 data points. Finally, it obtains a raw fault dataset which is a matrix of [13, 480000]. In this paper, the raw fault dataset is directly input into the input layer of the proposed CNN-GAP fault diagnosis model. According to Section 2.1, in the input layer of the proposed CNN-GAP model, some data process operations are performed including data normalization, data segmentation, data reconstruction, and data augmentation. Each raw 1-D long time-series data segment which has 480,000 data points is normalized firstly. The amplitude of each data segment is transformed into 0∼1. Then, according to Figure 5 and Formula 5, each long 1-D time-series data segment is segmented into 1599 short data segments by the overlap sampling data segmentation method. Here, each short data segment is a fault sample that contains 400 data points. The overlap rate is 25%, and the length of the stride is 300. To facilitate statistics, the first 1500 samples of each fault type are retained in this experiment. Finally, it obtains a new fault dataset which is a matrix of [13, 1500, 400]. Different fault sample has different fault label. The detail fault dataset is listed in Table 2. Figure 12 is the output voltage waveform of the isolated DC/DC inverter under the normal working state. Figure 13 is the output voltage waveform of 12 IGBT under the fault state. It can be seen from Figure 13, the output voltage fault waveform of the IGBT in the primary side (IGBT1∼IGBT6) is obviously different from the secondary side (IGBT7∼IGBT12). However, the fault waveforms of IGBTs on the same side are particularly similar and it is difficult to distinguish them.

To meet the data format requirement of the input layer in the proposed CNN-GAP, according to Section 2.1, each 1-D time-series data fault sample can be transformed into a 2-D feature map by the data reconstruction method shown in Figure 6. In Table 2, each 1-D time-series data (400, 1) are reconstructed into a 2-D input feature map form (20, 20, 1). Here, the first 20 represents the height of the feature map, the second 20 represents the width of the feature map, and 1 represents one channel. Therefore, each fault state has 1500 2-D input feature map sample data, as shown in Table 2. The input 2-D feature map of 12 faults is shown in Figure 14. Finally, the fault dataset is divided. All the

TABLE 2. The description of the fault dataset of the DC-DC inverter.

Fault label	Fault Type	Sample number	Sample length	Reshape into 2D feature map	One-hot Label
0	Normal	1500	400	[20, 20, 1]	[1,0,0,0,0,0,0,0,0,0,0,0,0]
1	LV-IGBT1 Open-circuit	1500	400	[20, 20, 1]	[0,1,0,0,0,0,0,0,0,0,0,0,0]
2	LV-IGBT2 Open-circuit	1500	400	[20, 20, 1]	[0,0,1,0,0,0,0,0,0,0,0,0,0]
3	LV-IGBT3 Open-circuit	1500	400	[20, 20, 1]	[0,0,0,1,0,0,0,0,0,0,0,0,0]
4	LV-IGBT4 Open-circuit	1500	400	[20, 20, 1]	[0,0,0,0,1,0,0,0,0,0,0,0,0]
5	LV-IGBT5 Open-circuit	1500	400	[20, 20, 1]	[0,0,0,0,0,1,0,0,0,0,0,0,0]
6	LV-IGBT6 Open-circuit	1500	400	[20, 20, 1]	[0,0,0,0,0,0,1,0,0,0,0,0,0]
7	HV-IGBT1 Open-circuit	1500	400	[20, 20, 1]	[0,0,0,0,0,0,0,1,0,0,0,0,0]
8	HV-IGBT2 Open-circuit	1500	400	[20, 20, 1]	[0,0,0,0,0,0,0,0,1,0,0,0,0]
9	HV-IGBT3 Open-circuit	1500	400	[20, 20, 1]	[0,0,0,0,0,0,0,0,0,1,0,0,0]
10	HV-IGBT4 Open-circuit	1500	400	[20, 20, 1]	[0,0,0,0,0,0,0,0,0,0,1,0,0]
11	HV-IGBT5 Open-circuit	1500	400	[20, 20, 1]	[0,0,0,0,0,0,0,0,0,0,0,1,0]
12	HV-IGBT6 Open-circuit	1500	400	[20, 20, 1]	[0,0,0,0,0,0,0,0,0,0,0,0,1]

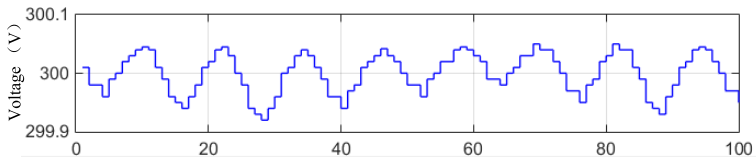

FIGURE 12. The output voltage waveform of DC/DC inverter under the normal working state.

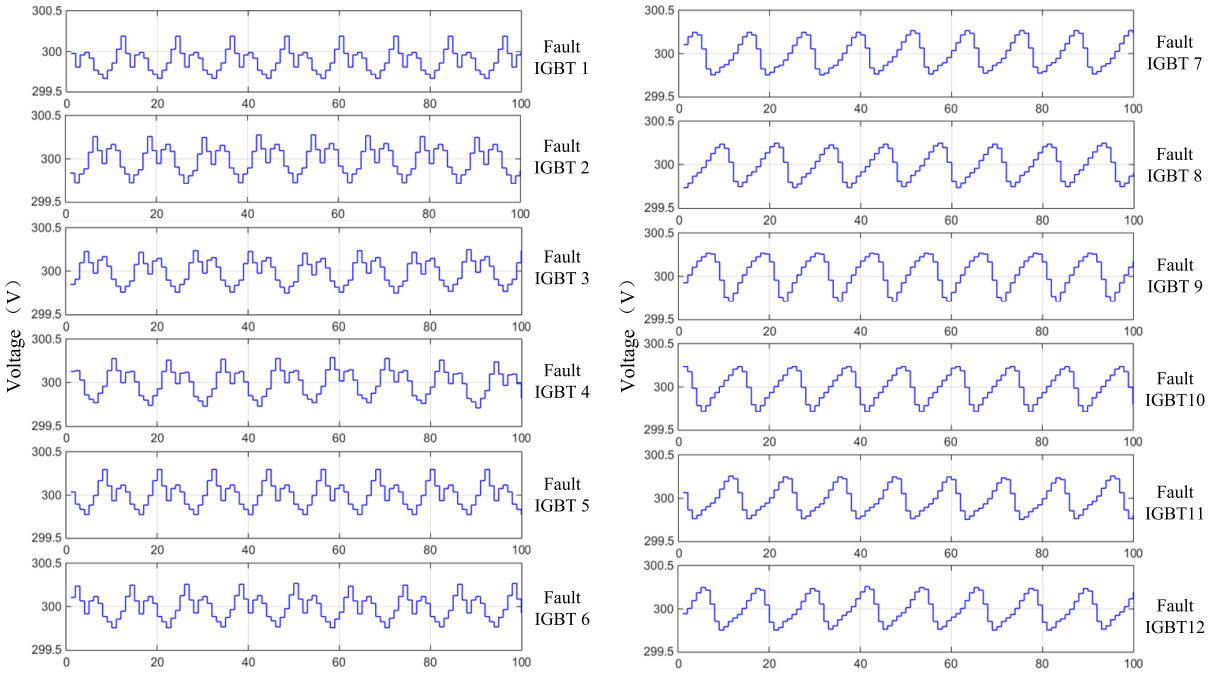

FIGURE 13. The output voltage waveform of the DC/DC inverter under the 12 faults state.

samples of each fault type are randomly divided into a training dataset, a validation dataset, and a test dataset. 30% of samples in each fault type (1500 samples) are randomly taken as a test dataset. In the remaining 70% of the samples, 80% are randomly selected as a training dataset and 20% are a validation dataset. In this experiment, the total sample quantity is 19500 (1500 × 13). The sample quantity of the total test dataset is 5850 (19500 × 0.3). The sample quantity of the total training dataset is 10920 (19500 × 0.7 × 0.8). The sample quantity of the total verification dataset is 2730 (19500 × 0.7 × 0.2).

In this paper, the training dataset is used for training the established CNN-GAP model. During the training process, the verification dataset is used for verifying the accuracy of the trained CNN-GAP model. Through repeated to adjust model parameters and testing, the hyper-parameter of the

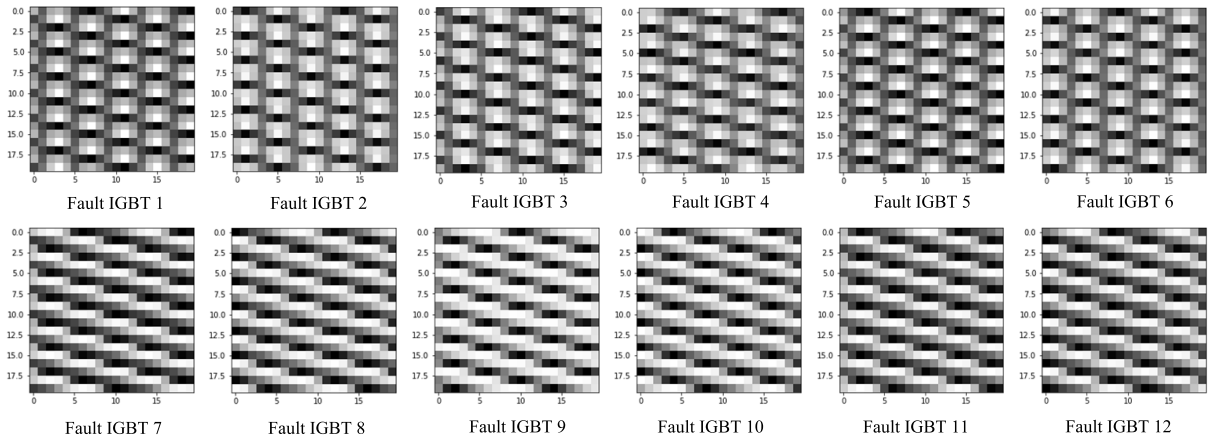

FIGURE 14. The 2-D feature map of DC/DC inverter under the 12 faults state.

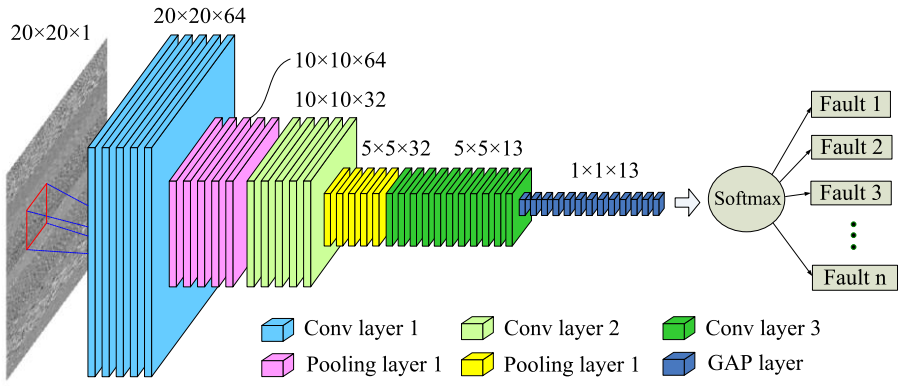

FIGURE 15. The structure of the improved CNN-GAP fault diagnosis model.

CNN-GAP model is compared and selected according to the precision curve of the verification dataset. The test dataset is used for the final fault classification and accuracy assessment of the trained CNN-GAP model. Finally, the new fault data is input into the trained CNN-GAP model. The fault feature of the raw input data is automatically extracted by using the trained CNN-GAP model. The final fault diagnosis classification result is automatically outputted.

C. HYPER-PARAMETERS OF THE ESTABLISHED CNN-GAP FAULT DIAGNOSIS MODEL

In general, different topology structures and hyper-parameters of the CNN model can obtain different diagnosis effect. Selecting the appropriate model hyper-parameters can effectively improve the fault diagnosis accuracy, training speed, and test speed [20]. The main model hyper-parameters include activation functions, optimizers, learning rates, convolution kernels, pooling kernels, and the CNN layer quantity, etc. Literature [20] gives a reference for hyper-parameter selection. According to the aforementioned research [20], in this section, the proposed intelligent fault diagnosis method based on the improved CNN-GAP model is established, as shown in Figure 15.

This model contains 3 convolution layers, 2 max-pooling layers, 1 global average pooling layer, and 1 Softmax layer. The detail hyper-parameters of the established CNN-GAP model are listed in Table 3. Firstly, the raw 2-D feature map is inputted into the first convolution layer of the improved CNN-GAP model. In the first convolution layer, there are 64 representative features are extracted from the raw input feature map. Each representative feature corresponds to an output feature map. Therefore, the output of the first convolution layer is a multi-dimensional tensor which has 64 channels. Behind the first convolutional layer is a max-pooling layer. By the max-pooling operation, the feature map could reduce by 75% of its original size. Behind the first pooling layer is the second convolutional layer. In the second convolution layer, there are 32 representative features are extracted from the output feature map of the first pooling layer. Behind the second convolutional layer is the second pooling layer. The size of each output feature map is further reduced. Behind the second pooling layer is the third convolutional layer. The output of the third convolutional layer is directly a 13 channels feature map. Behind the third convolutional layer is a global average pooling layer. The GAP layer has 13 global average pooling kernels. The output of the GAP layer is a 1-D array which has 13 values. Behind the GAP layer is a

TABLE 3. The hyper-parameters of the improved CNN-GAP model in the experiments.

Layer type	Hyper-parameter settings	Output shape	Parameter amount
Input layer	[batch, 20×20, 1]	[batch, 20×20, 1]	0
Convolution layer 1	Filter=[3×3, 1, 64], padding="Same", strides=[1, 1], "ReLU" activation function	[batch, 20×20, 64]	640
Max-Pooling layer 1	Ksize=[1, 2×2, 1], padding= "Same", strides =[2, 2]	[batch, 10×10, 64]	0
Dropout layer 1	Dropout (0.3)	[batch, 10×10, 64]	0
Convolution layer 2	Filter= [3×3, 64, 32], padding= "Same", strides =[1, 1], "ReLU" activation function	[batch, 10×10, 32]	18464
Max-Pooling layer 2	Ksize=[1, 2×2, 1], padding= "Same", strides =[2, 2]	[batch, 5×5, 32]	0
Dropout layer 2	Dropout (0.3)	[batch, 5×5, 32]	0
Convolution layer 3	Filter=[3×3, 32, 13], padding="Same", strides=[1,1], "ReLU" activation function	[batch, 5×5, 13]	3757
Global average pooling layer	Ksize= [1,5×5,1], padding= "Same", strides =[5, 5]	[batch, 1×1, 13]	0
Softmax output layer	Softmax activation function	[batch, 13]	0

TABLE 4. The detail hyper-parameters of the traditional CNN model in the experiments.

Layer type	Hyper-parameter settings	Output shape	Parameter amount
Input layer	[batch, 20×20, 1]	[batch, 20×20, 1]	0
Convolution layer 1	Filter=[3×3, 1, 64], padding="Same", strides=[1, 1], "ReLU" activation function	[batch, 20×20, 64]	640
Max-Pooling layer 1	Ksize=[1, 2×2, 1], padding= "Same", strides =[2, 2]	[batch, 10×10, 64]	0
Dropout layer 1	Dropout (0.3)	[batch, 10×10, 64]	0
Convolution layer 2	Filter= [3×3, 64, 32], padding= "Same", strides =[1, 1], "ReLU" activation function	[batch, 10×10, 32]	18464
Max-Pooling layer 2	Ksize=[1, 2×2, 1], padding= "Same", strides =[2, 2]	[batch, 5×5, 32]	0
Dropout layer 2	Dropout (0.3)	[batch, 5×5, 32]	0
Convolution layer 3	Filter=[3×3, 32, 13], padding="Same", strides=[1,1], "ReLU" activation function	[batch, 5×5, 13]	3757
Flatten layer	flatten Convolution layer 3 to 1-D shape	[batch, 325]	0
FC-Dense layer 1	256 hidden layer neuron nodes, "Tanh" activation function	[batch, 256]	83456
Dropout layer 3	Dropout (0.3)	[batch, 256]	0
FC-Dense layer 2	128 hidden layer neuron nodes, "Tanh" activation function	[batch, 128]	32896
Dropout layer 4	Dropout (0.3)	[batch, 128]	0
FC-Dense layer 3	13 hidden layer neuron nodes, "Tanh" activation function	[batch, 13]	1677
Softmax output layer	Softmax activation function	[batch, 13]	0

Softmax function. Finally, the classification results could be automatically output by the Softmax classifier.

In this experiment, the deep learning training skills including dropout technology, and batch normalization are applied in the training stage of the CNN-GAP model to prevent the model over-fitting problem. To improve the generalization ability and robustness of the trained CNN model, the data augmentation is applied in the model training process including the random cropping, left-right flipping, left rotation, average blurring, up-down flipping, and right rotation, etc. These operations are automatically performed by computer programs. The ReLU activation function is used in all convolutional layers. The optimizer is a very important selection to impact the convergence of the CNN model. In this experiment, the Adam adaptive learning rate optimization algorithm [20] is used. The learning rate can automatically adjust according to the local error surface of each epoch iteration. In this paper, the mini-batch training method is used. The number of samples in each mini-batch is set to 256. The iteration epoch is 50. To compare with the traditional CNN model, in this paper, a traditional CNN model with a fully connected layer is established. The detail hyper-parameters of the traditional CNN model are listed in Table 4. The traditional CNN model has the same model hyper-parameters

TABLE 5. The fault diagnosis results of the different CNN models.

Model name	Test accuracy	Training time (s)	testing time (s)
Traditional CNN model	99.23%	901.26	2.945
Improved CNN-GAP model	99.95%	824.89	2.488

to the improved CNN-GAP model in the feature extract layer. This comparison reference model has 3 fully connected hidden layers.

Compared with Table 3 and Table 4, the total parameter quantity of the traditional CNN diagnosis model using the fully connected layer of 3 layers is up to 140,890. However, the total parameter quantity of the improved CNN-GAP diagnosis model using the global average pooling layer is only 22,861. Therefore, the result shows that the improved CNN-GAP model can greatly reduce more than 80% trainable parameters quantity. The calculation method of the model parameter quantity in each network layer can refer to Formula 9 [20].

$$\begin{cases} \mathrm{CNN_{num}} = K_{num} \times k_{height} \times k_{width} \times I_{num} \times B_{num} \\ \mathrm{FCN_{num}} = N_{input} \times N_{output} \times B_{hidden} \end{cases} \tag{9}$$

where $\mathrm{CNN_{num}}$ is the parameter quantity of the convolution layer, $\mathrm{FCN_{num}}$ is the parameter quantity of the fully connected layer, K_{num} is the number of convolution kernels (the number of output channels), $k_{height} \times k_{width}$ represents the height $\times$ width of the convolution kernel, I_{num} is the number of input data channels, B_{num} is the number of biases of the convolutional layer, $N_{input} \times N_{output}$ represents the product of the number of neuron nodes between two adjacent layers in the fully connected layer, and B_{hidden} is the bias of the hidden layer. The max-pooling layer, dropout layer, and global average pooling layer have not any trainable parameters.

The diagnosis result and time cost of the improved CNN-GAP model and the traditional CNN model are listed in Table 5. As can be seen from Table 5, the effectiveness of the improved CNN-GAP model is obviously better than the traditional CNN model. In terms of time, the training time and test time of the improved CNN-GAP model is obviously faster than the traditional CNN model. The training time and test time of the traditional CNN are 901.26 seconds and 2.945 seconds respectively. However, the training time and test time of the improved CNN-GAP method are 824.89 seconds and 2.488 seconds respectively. In terms of accuracy, the test accuracy of the improved CNN-GAP model is better than the traditional CNN model. The accuracy rate of the traditional CNN model on the test dataset is 99.23%. The accuracy rate of the improved CNN-GAP on the test dataset is up to 99.95%. Therefore, the results confirm that the improved CNN-GAP method can effectively improve the diagnosis speed and test accuracy. The experiment is completed on the computer with Intel i5-2430 CPU, 8GB memory, NVIDIA GeForce GT 550M GPU, Tensorflow 1.10 version and Python 3.6.

D. THE FAULT DIAGNOSIS RESULT EVALUATION

It is meaningful to further evaluate and compare the classification performance of the improved CNN-GAP algorithm and the traditional CNN method or other methods. In the evaluation system of classifiers, F1-measure is a widely used criterion, which contains both the Precision ratio and the Recall ratio. The mathematical expressions of the three indicators are shown in Formula 10 [20]. Table 6 lists the precision rates, recall rates, and F1-score of the final diagnosis results (as shown in Table 5) of the improved CNN-GAP method and traditional CNN method.

$$\begin{cases} P = TP/(TP + FP) \times 100 \\ R = TP/(TP + FN) \times 100 \\ F_1 = 2TP/(2TP + FP + FN) \times 100 \end{cases} \tag{10}$$

where P is the precision rate, R is recall rate, F_1 is a harmonic average value of the precision rate and the recall rate, TP represents the number of true-positive instances, FP represents the number of false-positive instances, TP represents the number of true-positive instances, and FN represents the number of false-negative instances.

It can be seen from Table 6, the diagnosis accuracy of the improved CNN-GAP method is obviously better than the traditional CNN method. The F1-measure of the improved CNN-GAP is up to 99.95%, however, the traditional CNN method is 99.23%. Although it seems that there is not much difference in the results of the two methods, in fact, it is a great improvement. To further accurately locate and display the location and number of misclassification, a visualization method called multi-class confusion matrix [32] is introduced. The multi-class confusion matrix of the improved CNN-GAP method and traditional CNN method corresponding to the results of Table 6 is shown in Figure 16 (a) and Figure 16 (b) respectively.

In Figure 16, the abscissa axis of the multi-class confusion matrix represents the predicted category of the improved CNN-GAP. The ordinate axis represents the actual category label of the DC-DC inverter. The elements on the main diagonal represent the sample number of the correct classification of each fault state. As can be seen from Figure 16 (a), in the 5850 samples, only 3 samples are misclassified by the improved CNN-GAP prediction. The actual label of the misclassified sample is Fault 1, the predicted category of the CNN-GAP model is Fault 5 (2 samples) and Fault 6 (1 sample) respectively. Except for the recall rate of Fault 1 is 99.33%, the recall rates of other conditions are 100%. The diagnosis accurate of the normal state is 100%. As can be seen from Figure 16 (b), the traditional CNN method has 45 samples mistake classification. Among them, 12 Fault 1 are misjudged as Fault 3 (1 sample) and Fault 5 (11 samples). 33 Fault 7 are misjudged as Fault 11. The results show that the proposed CNN-GAP method has superior recognition ability and diagnostic accuracy than the traditional CNN method for the IGBT open-circuit fault of the DC-DC inverter.

TABLE 6. The evaluation results of the two different CNN model.

Health States	Improve CNN-GAP method			Traditional CNN model			Sample amount
	Precision rate	Recall rate	F1-measure	Precision rate	Recall rate	F1-measure	
Normal state	1.0000	1.0000	1.0000	1.0000	1.0000	1.0000	450
Fault 1	1.0000	0.9933	0.9967	1.0000	0.9733	0.9865	450
Fault 2	1.0000	1.0000	1.0000	1.0000	1.0000	1.0000	450
Fault 3	1.0000	1.0000	1.0000	0.9978	1.0000	0.9989	450
Fault 4	1.0000	1.0000	1.0000	1.0000	1.0000	1.0000	450
Fault 5	0.9956	1.0000	0.9978	0.9761	1.0000	0.9879	450
Fault 6	0.9978	1.0000	0.9989	1.0000	1.0000	1.0000	450
Fault 7	1.0000	1.0000	1.0000	1.0000	0.9267	0.9619	450
Fault 8	1.0000	1.0000	1.0000	1.0000	1.0000	1.0000	450
Fault 9	1.0000	1.0000	1.0000	1.0000	1.0000	1.0000	450
Fault 10	1.0000	1.0000	1.0000	1.0000	1.0000	1.0000	450
Fault 11	1.0000	1.0000	1.0000	0.9317	1.0000	0.9646	450
Fault 12	1.0000	1.0000	1.0000	1.0000	1.0000	1.0000	450
Average/total	0.9995	0.9995	0.9995	0.9927	0.9923	0.9923	5850

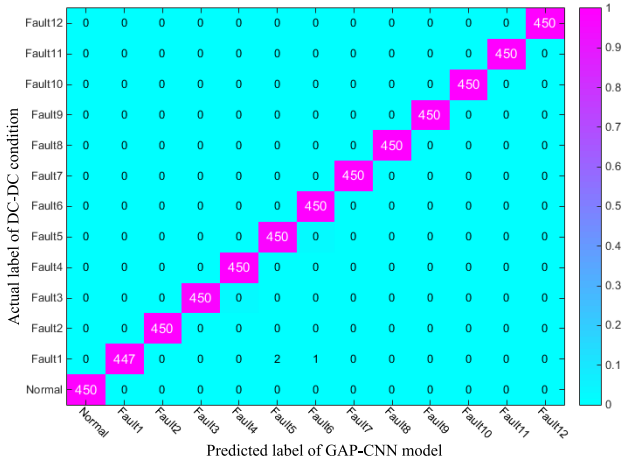

(a) The confusion matrix of the fault diagnosis results by using the proposed CNN-GAP method.

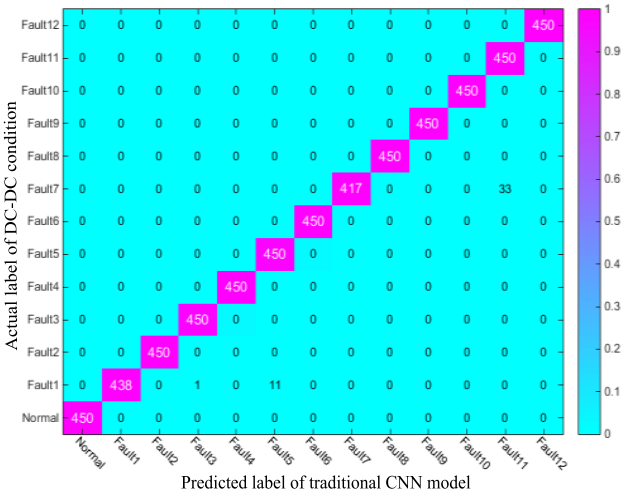

(b) The confusion matrix of the fault diagnosis results by using the traditional CNN method.

FIGURE 16. The multi-class confusion matrix of fault diagnosis results under different methods.

E. COMPARISON WITH TRADITIONAL INTELLIGENT METHODS

Totally different from the traditional methods, the proposed method focuses on the intelligent and fast fault diagnosis without any manual feature extraction. To further validate the superiority of the modified CNN-GAP algorithm than other traditional methods, in this paper, the three common mainstream traditional intelligent diagnosis algorithms are compared with the proposed method. The current mainstream intelligent diagnosis algorithms include the support vector machine (SVM), BP neural network (BPNN), K nearest neighbor (KNN), and deep BP neural network (DNN). In the traditional intelligent fault diagnosis methods, the manual feature extraction of the raw dataset is conducted firstly. Then, the extracted features are inputted into the intelligent diagnosis algorithm to complete the classification prediction [37]. Statistical features in the time domain and frequency domain are widely used method in fault diagnosis fields [41], [42]. Xia *et al.* [37] extracted 14 features from raw data by using 14 feature extraction operators, including 10 time-domain features and 4 frequency-domain features. The detailed feature parameters are listed in Table 7 [20]. This paper uses the 14 feature extraction operators to calculate the 14 statistical features of each fault sample of Table 2. Then, the extracted 14 features are input into SVM, KNN, and BPNN for fault diagnosis. The experimental results of the precision rate and the recall rate of the different methods are listed in Table 8.

Comparing Table 8, it can be seen the accuracy of the proposed CNN-GAP method is obviously better than other intelligent algorithms. In terms of accuracy, the precision rates of the SVM, KNN, and BPNN after manual feature extraction are 96.13%, 95.15%, 80.32% respectively. The precision rate of the DNN is 97.01% by using 5 hidden layers to train raw data. It can be seen in Table 8, the classification accuracy of

TABLE 7. The statistical feature extractions in the time-domain and frequency-domain.

Domain	Feature parameters	
Time-domain	Absolute mean: $\frac{1}{n}\sum_{i=1}^{n}\lvert x_i\rvert$	Crest factor: $\max\left(\lvert x_i\rvert\right)/\sqrt{\frac{1}{n}\sum_{i=1}^{n}x_i^2}$
	Variance: $\frac{1}{n}\sum_{i=1}^{n}\left(x_i-\bar{x}\right)^2$	Root mean square: $\sqrt{\frac{1}{n}\sum_{i=1}^{n}x_i^2}$
	Crest: $\max\left(\lvert x_i\rvert\right)$	Pulse factor: $\max\left(\lvert x_i\rvert\right)/\left(\frac{1}{n}\sum_{i=1}^{n}\lvert x_i\rvert\right)$
	Clearance factor: $\max\left(\lvert x_i\rvert\right)/\left(\frac{1}{n}\sum_{i=1}^{n}\sqrt{x_i^2}\right)^2$	Skewness: $\frac{1}{n}\sum_{i=1}^{n}x_i^3$
	Kurtosis: $\frac{1}{n}\sum_{i=1}^{n}x_i^4$	Shape factor: $\sqrt{\frac{1}{n}\sum_{i=1}^{n}x_i^2}/\left(\frac{1}{n}\sum_{i=1}^{n}\lvert x_i\rvert\right)$
Frequency-domain	Crest: $\max\left(\lvert X_i\rvert\right)$	Mean energy: $\frac{1}{n}\sum_{i=1}^{n}X_i$
	Kurtosis: $\frac{1}{n}\sum_{i=1}^{n}X_i^4$	Variance: $\frac{1}{n}\sum_{i=1}^{n}\left(X_i-\bar{X}\right)^2$

TABLE 8. The precision rate and recall rate of different methods.

Methods	CNN-GAP		SVM		KNN		BPNN		DNN		CNN	
Training time (s)	824.89		22.79		0.043		78.19		396.5		901.26	
Testing time (s)	2.488		4.139		0.074		0.050		0.271		2.945	
Health condition	*P* (%)	*R* (%)	*P* (%)	*R* (%)	*P* (%)	*R* (%)	*P* (%)	*R* (%)	*P* (%)	*R* (%)	*P* (%)	*R* (%)
Normal state	100	100	100	100	100	100	100	100	100	100	100	100
Fault 1	100	99.33	95.02	92.23	95.13	94.33	92.79	43.28	100	96.89	100	97.33
Fault 2	100	100	98.47	98.90	96.32	97.59	99.67	67.11	100	100	100	100
Fault 3	100	100	98.23	99.78	95.26	99.10	74.58	100	100	100	99.78	100
Fault 4	100	100	96.58	99.06	93.76	98.59	63.73	100	100	100	100	100
Fault 5	99.56	100	98.59	91.72	98.34	90.41	100	89.11	96.98	100	97.61	100
Fault 6	99.78	100	99.32	100	99.32	100	97.99	100	100	100	100	100
Fault 7	100	100	97.28	89.95	97.38	93.38	42.88	65.30	67.22	99.33	100	92.67
Fault 8	100	100	88.48	93.56	96.02	88.74	66.03	55.40	98.25	100	100	100
Fault 9	100	100	100	98.90	98.24	98.02	73.09	96.70	100	100	100	100
Fault 10	100	100	95.96	99.12	96.53	97.80	84.25	74.07	100	100	100	100
Fault 11	100	100	93.09	87.27	84.42	86.57	84.69	38.43	98.72	51.56	93.17	100
Fault 12	100	100	88.70	97.68	86.23	91.14	62.01	66.46	100	98.22	100	100
Average	99.95	99.95	96.13	96.03	95.15	95.06	80.32	76.51	97.01	95.85	99.27	99.23

all methods in normal samples is 100%. However, as for fault samples, only 2 hidden layers of BPNN have the lowest test accuracy and serious over-fitting. Because of the shallow network structure of the SVM, KNN, and BPNN, their diagnostic accuracy is difficult to further improve. When the number of DNN layer exceeds 5 layers, the accuracy of the DNN is difficult to increase because of the gradient disappearance and the over-fitting of the model is gradual obviousness. Comparing the results of the above six algorithms, it can be confirmed that the proposed CNN-GAP algorithm has more accurate and superior performance than other intelligent methods.

The main parameters of other methods are described as follows: (1) SVM: the penalty factor C = 10, kernel function is Gaussian radial basis function (RBF), and slack variable $\xi = 0.01$; (2) KNN: using the Minkowski distance, the k value is 3 and the leaf node is 30; (3) BPNN: the architecture is 14-256–128–13, the Adam adaptive learning rate optimization algorithm is used, the activation function is Tanh, the regularization coefficient $\lambda = 0.001$, the batch size is 256, and the iteration epoch is 300; and (4) DNN: the architecture is 400–512–256–128–64–13, which is decided by repeated trial experiences and guiding principles, the Adam optimization algorithm is used, the activation function is Tanh, the regularization coefficient $\lambda = 0.001$, the batch size is 256, and the iteration epoch is 300.

F. VISUALIZATION OF LEARNED FEATURE REPRESENTATION

In the above research result, this paper shows that the improved CNN-GAP model has the outstanding feature ability to learn representative features from raw fault data. However, it can not show how to learn these features. Consequently, in order to explain the black box operation process, a visualization method called t-distributed stochastic neighbor embedding (t-SNE) [33] is used. The t-SNE is a manifold learning algorithm. It is an effective method to visualize high-dimensional data by mapping the data samples from their raw feature space into a two or three-dimensional space map [28].

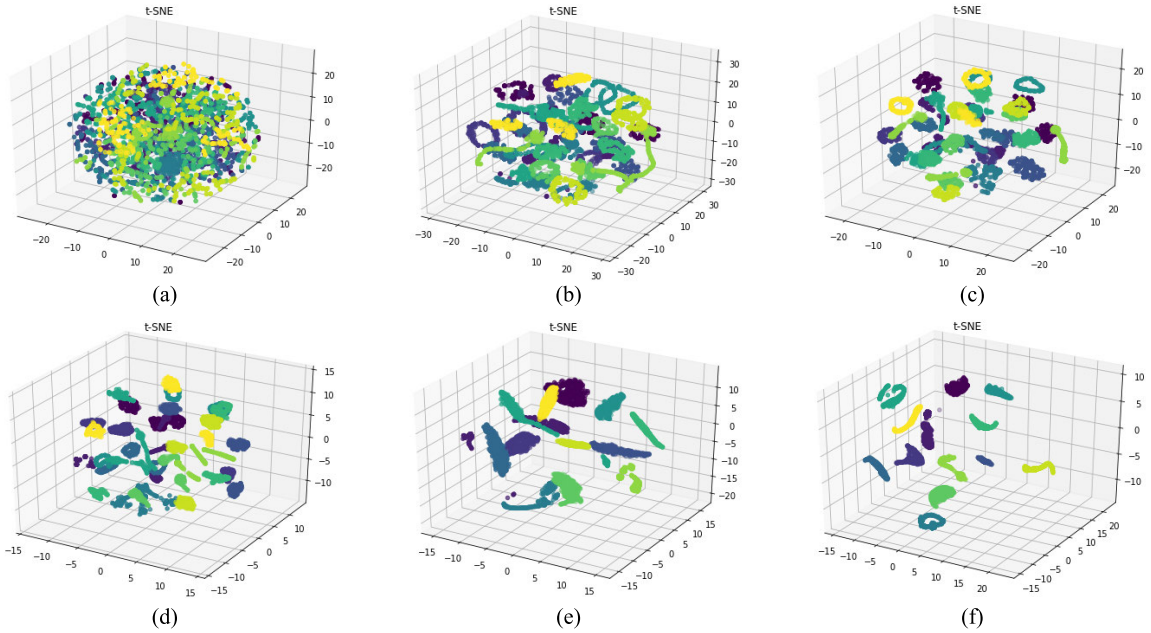

FIGURE 17. Scatter plots of the feature visualization under the test dataset using the t-SNE method. (a) The feature distribution of raw data, (b) the feature distribution of the convolutional layer 1, (c) the feature distribution of the convolutional layer 2, (d) the feature distribution of the convolutional layer 3, (e) the feature distribution of the global average pooling layer, (f) the feature distribution of the Softmax output layer.

Assuming that the parameter sets of the extracted feature sample is $\boldsymbol{F} = [f_1, \ f_2, \ \ldots, f_m]^T$, where $f_i = [f_{i1}, \ f_{i2}, \ \ldots, f_{in}]$, $i = 1, 2, \ldots$ m, m is the number of samples; where $i \in R^n$(n denotes the dimensional of the sample). The t-SNE aims to learn a map $\boldsymbol{P}$ (e.g., a Euclidean distance map) to transform $\boldsymbol{F}$ into a low dimensional embedding $\boldsymbol{L} = [l_1, \ l_2, \ \ldots, l_m]^T$, where $l_i \in R^s$(s denotes the embedding dimensions and usually $s = 2$ or 3). In order to learn the map $\boldsymbol{L}$, t-SNE firstly measures the pairwise similarity of the elements in $\boldsymbol{F}$ by Formula 11 [42].

$$\begin{cases} p_{j|i} = \dfrac{\exp(-\boldsymbol{P}(f_i, \ f_j)^2/2\sigma_i^2)}{\sum_{k \neq i} \exp(-\boldsymbol{P}(f_i, \ f_k)^2)/2\sigma_i^2}, & \text{and } p_{i|i} = 0 \\ p_{ij} = (p_{i|j} + p_{j|i})/2m \end{cases} \tag{11}$$

where p_{ij} and $p_{j|i}$ are the joint and the conditional probability between f_i and f_j, and σ_i is the bandwidth of the Gaussian kernels. Then, t-SNE computes the pairwise similarity of the elements in $\boldsymbol{L}$ by Formula 12.

$$\tilde{p}_{ij} = \frac{\left(1 + ||l_i - l_j||^2\right)^{-1}}{\sum_{k \neq h} \left(1 + ||l_k - l_h||^2\right)^{-1}}, \quad \text{and } \tilde{p}_{ij} = 0 \tag{12}$$

where is $\tilde{p}_{ij}$ the joint probability between l_i and l_j. Lastly, the location of the embedding element l_i will be determined by optimizing the Kullback-Leibler divergence between the joint distributions p_{ij} and $\tilde{p}_{ij}$. This paper uses 3-D space visualization, so $s = 3$. In this experiment, the 5850 samples of test datasets are as input data to input into the t-SNE. The data feature distribution of each layer after a dimensionality reduction by the t-SNE method is shown in Figure 17.

Figure 17(a)–(f) show the data feature distribution visualization of the input layer, the convolutional layer 1, convolutional layer 2, convolutional layer 3, the global average pooling layer, the Softmax output layer respectively. It can be obviously seen from Figure 17 (a)–(f), in the input layer, the 13 health states of the DC-DC inverter are very confusing. In convolutional layer 1, the different fault state has a slight distinction. In the convolutional layer 2, convolutional layer 3 and the global average pooling layer, the feature extraction ability of each layer is gradually increased. Finally, after the Softmax function is calculated, the 13-class health status data of the DC-DC inverter is clearly classified. As can be seen from Figure 17 (f), a few samples are still misclassified, which is consistent with the result of the confusion matrix of Figure 16 (a). The classification visualization obviously shows that the trained CNN-GAP model has an outstanding feature extraction ability and nonlinear mapping ability.

In the modern electrical power system, the open-circuit fault diagnosis of the DC-DC inverter is always an intractable and difficult problem. In this paper, the main purpose is to explore a novel fault diagnosis method based on the modified GAP-CNN algorithm for fast fault diagnosis of the DC-DC inverter. In this paper, the simulation data of the DC-DC inverter is used. Comparing with the actual DC-DC inverter, the simulation model of DC-DC inverter may generate some difference of output voltage waveform under the interference from the working environment to some extent. However, the deep learning-based fault diagnosis model has superior self-adaption on the real industrial data. One of the most important advantages of the CNN model is that they can automatically learn the representative features and the complex nonlinear relationships from the raw data In the actual industrial application, the proposed method still can automatically process the raw 1D time-series industrial data according to the proposed procedure in Section III. The end-to-end model

structure of the proposed method will obtain better operability and versatility on real industrial applications.

V. CONCLUSION

Fault diagnosis and health monitoring technology based on artificial intelligence is gradually widely used in electronic and electrical equipment. The traditional intelligent fault diagnosis method based on manual feature extraction extremely relies on the experience of engineers, and it is difficult to identify the micro features of the early-term faults. Convolutional neural network (CNN) has powerful feature extract ability which has the potential to extract the micro fault features. However, the fully connected layer structure of the traditional CNN has numerous trainable parameters which are not suitable for rapid diagnosing and real-time detecting of the incipient fault. In this paper, a novel deep learning model named improved CNN-GAP is proposed. This method is developed for fast fault diagnosis of the IGBT open-circuit fault in the DC-DC inverter. The proposed approach improves the model structure of the traditional CNN by using a global average pooling layer instead of the 2∼3 layers fully connected layer. The trainable parameter quantity of the traditional CNN model is greatly reduced by using the proposed improved method. The improved CNN-GAP method is mainly composed of an input layer, a feature extraction layer, a global average layer, and a Softmax output layer. The proposed method can directly learn features from raw 1-D time-series data without any time-consuming manual feature extraction and signal processing operations.

The proposed method is applied to address the intelligent fault diagnosis problem of the IGBT's open-circuit fault in the DC-DC inverter. The experiment result confirms the proposed method is more effective than other existing intelligence diagnosis methods including the SVM, KNN, BPNN, DNN, and traditional CNN. The experiment results show that the diagnostic accuracy is up to 99.95%, and the testing time can reduce by more than 15%. The improved CNN-GAP method could greatly reduce the model parameter quantity of the traditional CNN more than 80%, which is more suitable for rapid fault diagnosis and real-time online anomaly detection in electronic devices. The results confirmed that the proposed CNN-GAP algorithm has more accurate and superior diagnosis performance than other intelligent methods. The proposed method needs not any manual feature extraction and feature selection in raw 1-D time-series signals data. In this paper, the data augmentation and overlap sampling method are used to expand the number of fault samples. The multi-class confusion matrix and the t-SNE visualization method are used to further explain the classification performance of the CNN-GAP model. The end-to-end model structure of the proposed method has better operability and versatility on other applications. It is very interesting to develop other deep learning methods for intelligent fault diagnosis fields. The authors would further research this topic in the future.

AUTHOR CONTRIBUTIONS

W.G., H.C., and M.Z. contributed to conceiving the research idea and developed the algorithm and procedure. W.G. and Z.Z. conducted the establishment of the model, the calculation, and manuscript writing. M.Z. helped in analyzing the data, editing the manuscript and in the modification of the English grammar of the manuscript. H.G. contributed some useful suggestions and involved in the preparation of the manuscript. H.C. reviewed the manuscript and supervised the whole project. All authors contributed to discussing and analyzing the results.

REFERENCES

[1] M. H. Khooban, M. Gheisarnejad, and H. Farsizadeh, "A new intelligent hybrid control approach for DC–DC converters in zero-emission ferry ships," *IEEE Trans. Power Electron.*, vol. 35, no. 6, pp. 5832–5841, Jun. 2000.
[2] M. Mutarraf, Y. Terriche, K. Niazi, J. Vasquez, and J. Guerrero, "Energy storage systems for shipboard Microgrids—A review," *Energies*, vol. 11, no. 12, p. 3492, 3492.
[3] R. G. Wright, "Intelligent autonomous ship navigation using multi-sensor modalities," *TransNav, Int. J. Mar. Navigat. Saf. Sea Transp.*, vol. 13, no. 3, pp. 503–510, 2019.
[4] F. C. Robert, G. S. Sisodia, and S. Gopalan, "A critical review on the utilization of storage and demand response for the implementation of renewable energy microgrids," *Sustain. Cities Soc.*, vol. 40, pp. 735–745, Jul. 2018.
[5] N. Kai, Y. Hu, and X. Li, "An Overview of Design, Control, Power Management, System Stability and Reliability in Electric Ships," *Power Electron. Drives*, vol. 2017, vol. 2, no. 2, pp. 5–29.
[6] F. Balsamo, D. Lauria, and F. Mottola, "Design and control of coupled inductor DC–DC converters for MVDC ship power systems," *Energies*, vol. 12, no. 4, p. 751, 2019.
[7] F. Sun, J. Liu, F. Xiao, P. Chen, and X. Li, "An isolated bidirectional modular multilevel DC-DC converter for MVDC distribution system in ship," in *Proc. IEEE Int. Power Electron. Appl. Conf. Expo. (PEAC)*, Nov. 2018, pp. 1–6.
[8] X. Dianguo, L. Xiaofeng, and Y. Yong, "A survey on fault diagnosis and tolerant control of inverters," *Trans. China Electrotechn. Soc.*, vol. 30, no. 21, pp. 1–12, 2015.
[9] Z. Chen, Y. Chen, L. Wu, S. Cheng, and P. Lin, "Deep residual network based fault detection and diagnosis of photovoltaic arrays using current-voltage curves and ambient conditions," *Energy Convers. Manage.*, vol. 198, Oct. 2019, Art. no. 111793.
[10] M. Babaei, J. Shi, and S. Abdelwahed, "A survey on fault detection, isolation, and reconfiguration methods in electric ship power systems," *IEEE Access*, vol. 6, pp. 9430–9441, 2018.
[11] D. Espinoza Trejo, E. Bárcenas, J. Hernández Díez, G. Bossio, G. Espinosa, and Pérez, "Open- and short-circuit fault identification for a boost DC/DC converter in PV MPPT systems," *Energies*, vol. 11, no. 3, p. 616, 2018.
[12] S. Yang, D. Xiang, A. Bryant, P. Mawby, L. Ran, and P. Tavner, "Condition monitoring for device reliability in power electronic converters: A review," *IEEE Trans. Power Electron.*, vol. 25, no. 11, pp. 2734–2752, Nov. 2010.
[13] B. Lu and S. K. A. Sharma, "Literature review of IGBT fault diagnostic and protection methods for power inverters," *IEEE Trans. Ind. Appl.*, vol. 45, no. 5, pp. 1770–1777, Dec. 2009.
[14] Y. Yong, J. Shengcheng, and Y. Rongfeng, "IGBT open circuit fault diagnosis method for inverter," *Proc. CSEE*, vol. 31, no. 09, pp. 30–35, 2011.
[15] J. Poon, P. Jain, I. C. Konstantakopoulos, C. Spanos, S. K. Panda, and S. R. Sanders, "Model-based fault detection and identification for switching power converters," *IEEE Trans. Power Electron.*, vol. 32, no. 2, pp. 1419–1430, Feb. 2017.
[16] M. Alavi, D. Wang, and M. Luo, "Short-circuit fault diagnosis for three-phase inverters based on voltage-space patterns," *IEEE Trans. Ind. Electron.*, vol. 61, no. 10, pp. 5558–5569, Oct. 2014.
[17] K. Wawryn and W. Zinka, "A prototype expert system for fault diagnosis in electronic devices," in *Proc. Eur. Conf. Circuit Theory Design*, 1989, pp. 677–680.

[18] T. Wang, J. Qi, H. Xu, Y. Wang, L. Liu, and D. Gao, "Fault diagnosis method based on FFT-RPCA-SVM for cascaded-multilevel inverter," *ISA Trans.*, vol. 60, pp. 156–163, Jan. 2016.
[19] S. S. Moosavi, A. N'Diaye, A. Djerdir, Y. Ait-Amirat, and D. A. Khaburi, "Artificial neural network-based fault diagnosis in the AC–DC converter of the power supply of series hybrid electric vehicle," *IET Electr. Syst. Transp.*, vol. 6, no. 2, pp. 96–106, Jun. 2016.
[20] W. Gong, H. Chen, Z. Zhang, M. Zhang, R. Wang, C. Guan, and Q. Wang, "A novel deep learning method for intelligent fault diagnosis of rotating machinery based on improved CNN-SVM and multichannel data fusion," *Sensors*, vol. 19, no. 7, p. 1693, 1693.
[21] C. L. Wen, F. Y. Lv, Z. J. Bao, and M. Q. Liu, "A review of data driven-based incipient fault diagnosis," *J. Automatica Sinica*, vol. 42, no. 9, pp. 1285–1299, Sep. 2016.
[22] Z. Chen, L. Wu, S. Cheng, P. Lin, Y. Wu, and W. Lin, "Intelligent fault diagnosis of photovoltaic arrays based on optimized kernel extreme learning machine and I-V characteristics," *Appl. Energy*, vol. 204, pp. 912–931, Oct. 2017.
[23] Q. Sun, Y. Wang, and Y. Jiang, "A novel fault diagnostic approach for DC-DC converters based on CSA-DBN," *IEEE Access*, vol. 6, pp. 6273–6285, 2018.
[24] G. Wang, Y. Guan, J. Zhang, L. Wu, X. Zheng, and W. Pan, "ESR estimation method for DC-DC converters based on improved EMD algorithm," in *Proc. IEEE Prognostics Syst. Health Manage. Conf.*, May 2012, pp. 1–6.
[25] Q. Sun, Y. Wang, Y. Jiang, L. Shao, and D. Chen, "Fault diagnosis of SEPIC converters based on PSO-DBN and wavelet packet energy spectrum," in *Proc. Prognostics Syst. Health Manage. Conf. (PHM-Harbin)*, Jul. 2017, pp. 1–7.
[26] G. E. Hinton, "Reducing the dimensionality of data with neural networks," *Science*, vol. 313, no. 5786, pp. 504–507, Jul. 2006.
[27] L.-H. Wang, X.-P. Zhao, J.-X. Wu, Y.-Y. Xie, and Y.-H. Zhang, "Motor fault diagnosis based on short-time Fourier transform and convolutional neural network," *Chin. J. Mech. Eng.*, vol. 30, no. 6, pp. 1357–1368, Nov. 2017.
[28] W. Sun, R. Zhao, R. Yan, S. Shao, and X. Chen, "Convolutional discriminative feature learning for induction motor fault diagnosis," *IEEE Trans. Ind. Informat.*, vol. 13, no. 3, pp. 1350–1359, Jun. 2017.
[29] M. Lin, Q. Chen, and S. C. Yan, "Network in network," in *Proc. Int. Conf. Learn. Represent.*, 2014, pp. 1–10.
[30] I. Goodfellow, Y. Bengio, and A. Courville, *Deep Learning*. Cambridge, MA, USA: MIT Press, 2016.
[31] Y. Lecun, L. Bottou, Y. Bengio, and P. Haffner, "Gradient-based learning applied to document recognition," *Proc. IEEE*, vol. 86, no. 11, pp. 2278–2324, Aug. 1998.
[32] L. Wen, X. Li, L. Gao, and Y. Zhang, "A new convolutional neural network-based data-driven fault diagnosis method," *IEEE Trans. Ind. Electron.*, vol. 65, no. 7, pp. 5990–5998, Jul. 2018.
[33] W. Zhang, G. Peng, and C. Li, "A new deep learning model for fault diagnosis with good anti-noise and domain adaptation ability on raw vibration signals," *Sensors*, vol. 2017, vol. 17, no. 2, p. 425.
[34] Y. Liu, X. Yan, C.-A. Zhang, and W. Liu, "An ensemble convolutional neural networks for bearing fault diagnosis using multi-sensor data," *Sensors*, vol. 19, no. 23, p. 5300, 2019.
[35] D. M. Montserrat, Q. Lin, J. Allebach, and E. Delp, "Training object detection and recognition CNN models using data augmentation," *Electron. Imag.*, vol. 2017, no. 10, pp. 27–36, Jan. 2017.
[36] D. Han, Q. Liu, and W. Fan, "A new image classification method using CNN transfer learning and Web data augmentation," *Expert Syst. Appl.*, vol. 95, pp. 43–56, Apr. 2018.
[37] M. Xia, T. Li, L. Xu, L. Liu, and C. W. de Silva, "Fault diagnosis for rotating machinery using multiple sensors and convolutional neural networks," *IEEE/ASME Trans. Mechatronics*, vol. 23, no. 1, pp. 101–110, Feb. 2018.
[38] D. P. Kingma and J. Ba, "Adam: A method for stochastic optimization," 2014, *arXiv:1412.6980*. [Online]. Available: http://arxiv.org/abs/1412.6980
[39] L. Luyao, *Research on Typical Topologies of Dual Active Bridge Bidirectional DC-DC Converter*. Beijing, China: Beijing Jiaotong Univ., 2016.
[40] Z. Xuan, H. Shenghua, and N. Guoyun, "A three-phase dual active bridge bidirectional ZVS DC/DC converter," *Phys. Procedia*, vol. 24, pp. 139–148, Dec. 2012.
[41] X. Guo, L. Chen, and C. Shen, "Hierarchical adaptive deep convolution neural network and its application to bearing fault diagnosis," *Measurement*, vol. 93, pp. 490–502, Nov. 2016.
[42] W. Xi, Z. Li, Z. Tian, and Z. Duan, "A feature extraction and visualization method for fault detection of marine diesel engines," *Measurement*, vol. 116, pp. 429–437, Feb. 2018.

WENFENG GONG was born in Shandong, China, in January 1987. He received the B.S. degree in mechanical engineering from the Shandong University of Science and Technology, Taian, China, in 2009, and the M.S. degree in mechanical engineering from the Guilin University of Electronic and Technology, Guilin, China, in 2014. He is currently pursuing the Ph.D. degree in marine engineering with the School of Energy and Power Engineering, Wuhan University of Technology, Wuhan, China.

He is also a Co-Cultivating Doctorate with Nanyang Technological University, Singapore, with funding from the China Scholarship Council. He had published more than 15 research articles. He holds three Chinese invention patents and more than 30 Chinese utility model patents. His research interests include intelligent fault diagnosis, health condition monitoring in mechanical and electrical equipment, deep learning, and machine learning.

HUI CHEN received the B.S. and M.S. degrees in power machinery and engineering, and the Ph.D. degree in marine engineering from the Wuhan University of Technology, Wuhan, China, in 1984, 1987, and 1991, respectively.

He is currently a Professor with the Center for System Simulation and Control Engineering, Wuhan University of Technology, in May 2000. His current research interests include ship electrical propulsion modeling, control and fault diagnosis, and ship power management and control.

ZEHUI ZHANG was born in Shandong, China, in September 1994. He received the B.S. degree in marine engineering from Shanghai Maritime University, Shanghai, China, in 2016, and the M.S. degree from the Wuhan University of Technology, Wuhan, China, in 2019. He is currently pursuing the Ph.D. degree with the College of Software, Nankai University, Tianjin, China.

His current research interests include computer vision and intelligent control.

MEILING ZHANG was born in Hunan, China, in October 1987. She received the B.S. degree in computer network technology from Hunan Agricultural University, Changsha, China, in 2009, and the M.S. degree in project management engineering from the Guilin University of Electronic and Technology, Guilin, China, in 2014.

She is currently an Associate Professor with the Beihai Campus, Guilin University of Electronic and Technology. She has published more than ten teaching and research articles. Her research interests include artificial neural networks, data statistical analysis, blockchain, financial audit, and risk assessment.

HAIBO GAO is currently an Associate Professor with the School of Energy and Power Engineering, Wuhan University of Technology, Wuhan, China. His current research interests include performance simulation of marine electric propulsion systems and fault diagnosis of marine engineering systems.